AWARD NUMBER: W81XWH-19-1-0478

TITLE: A Microfluidic Method to Define the Role of Skin Microenvironment in Melanomagenesis

PRINCIPAL INVESTIGATOR: Vijayasaradhi Setaluri

CONTRACTING ORGANIZATION: The Board of Regents of the University of Wisconsin System

REPORT DATE: October 2020

TYPE OF REPORT: Annual

PREPARED FOR: U.S. Army Medical Research and Development Command
Fort Detrick, Maryland 21702-5012

DISTRIBUTION STATEMENT: Approved for Public Release;
Distribution Unlimited

# REPORT DOCUMENTATION PAGE

*Form Approved*
*OMB No. 0704-0188*



| 1. REPORT DATE | 2. REPORT TYPE | 3. DATES COVERED |
|---|---|---|
| Oct 2020 | Annual | 09/01/2019-08/31/2020 |

**4. TITLE AND SUBTITLE**

A Microfluidic Method to Define the Role of Skin Microenvironment in Melanomagenesis

**5a. CONTRACT NUMBER**

**5b. GRANT NUMBER**
**W81XWH-19-1-0478**

**5c. PROGRAM ELEMENT NUMBER**

**6. AUTHOR(S)**

VIJAYASARADHI SETALURI

E-Mail: VSETALURI@DERMATOLOGY.WISC.EDU

**5d. PROJECT NUMBER**

**5e. TASK NUMBER**

**5f. WORK UNIT NUMBER**

**7. PERFORMING ORGANIZATION NAME(S) AND ADDRESS(ES)**

University of Wisconsin-Madison

**8. PERFORMING ORGANIZATION REPORT NUMBER**

**9. SPONSORING / MONITORING AGENCY NAME(S) AND ADDRESS(ES)**

U.S. Army Medical Research and Development Command
Fort Detrick, Maryland 21702-5012

**10. SPONSOR/MONITOR'S ACRONYM(S)**

**11. SPONSOR/MONITOR'S REPORT NUMBER(S)**

**12. DISTRIBUTION / AVAILABILITY STATEMENT**

Approved for Public Release; Distribution Unlimited

**13. SUPPLEMENTARY NOTES**

**14. ABSTRACT**

Exposure to environmental UV radiation (UVR) is considered a major etiological factor for skin cancer including malignant melanoma, the deadliest form of skin cancer. Since the ambient UVR exposure is greatest during midday hours, tasks such as long periods of training exercises for soldiers or sailors can influence the daily UVR exposure. Deployment of military personnel over the past decade in countries with near maximum annual averages of solar radiation potentially increases their risk of melanoma. Mutations in genes (specifically NRAS and BRAF) that activate mitogen activated protein kinase signaling are the major drivers of cutaneous melanoma and found in >80% melanomas. Majority of nevi, which are collections of growth arrested melanocytes, also harbor mutations in BRAF, but do not necessarily act as precursors of melanoma. A widely accepted explanation for this observation is that melanocytes that acquire oncogenic mutations proliferate transiently and then are growth arrested due to oncogene-induced senescence (OIS), which acts as barrier to melanoma development. Bypass or escape from OIS is thought to be responsible for melanoma tumor development from BRAF-transformed melanocytes. Efforts to validate the OIS model produced conflicting data. While investigations were primarily focused on genetic and epigenetic events within melanocytes, the role skin microenvironment plays in OIS is poorly understood.The overall goal of this project is to understand the role of melanocyte microenvironment in melanoma tumor development. We hypothesize that cellular contact with UV exposed epidermal keratinocytes and/or secreted factors from other skin-resident cells influence OIS-escape and malignant melanoma tumor development. Genetic mouse models and co-culture of isolated human skin cell, although useful, have several limitations. Microfluidic methods offer powerful and versatile alternative to overcome the limitations of these approaches. We will test the hypothesis that skin microenvironment plays a role in melanoma development by employing freshly isolated melanocytes, keratinocytes and fibroblasts on a microfluidic platform.

**15. SUBJECT TERMS**

| 16. SECURITY CLASSIFICATION OF: | | | 17. LIMITATION OF ABSTRACT | 18. NUMBER OF PAGES | 19a. NAME OF RESPONSIBLE PERSON |
|---|---|---|---|---|---|
| a. REPORT | b. ABSTRACT | c. THIS PAGE | | | USAMRMC |
| Unclassified | Unclassified | Unclassified | Unclassified | | 19b. TELEPHONE NUMBER *(include area code)* |

**Standard Form 298 (Rev. 8-98)**
**Prescribed by ANSI Std. Z39.18**

## TABLE OF CONTENTS


| | Page |
|---|---|
| 1. Introduction | 4 |
| 2. Keywords | 4 |
| 3. Accomplishments | 5-14 |
| 4. Impact | 15 |
| 5. Changes/Problems | 15-16 |
| 6. Products | 16 |
| 7. Participants & Other Collaborating Organizations | 16 |
| 8. Special Reporting Requirements | 17 |
| 9. Appendices | 18-40 |

**INTRODUCTION:** *Narrative that briefly (one paragraph) describes the subject, purpose and scope of the research.*

Exposure to environmental UV radiation (UVR) is considered a major etiological factor for skin cancer including malignant melanoma, the deadliest form of skin cancer. Since the ambient UVR exposure is greatest during midday hours, tasks such as long periods of training exercises for soldiers or sailors can influence the daily UVR exposure. Deployment of military personnel over the past decade in countries with near maximum annual averages of solar radiation potentially increases their risk of melanoma. Mutations in genes (specifically NRAS and BRAF) that activate mitogen activated protein kinase signaling are the major drivers of cutaneous melanoma and found in >80% melanomas. Majority of nevi, which are collections of growth arrested melanocytes, also harbor mutations in BRAF, but do not necessarily act as precursors of melanoma. A widely accepted explanation for this observation is that melanocytes that acquire oncogenic mutations proliferate transiently and then are growth arrested due to oncogene-induced senescence (OIS), which acts as barrier to melanoma development. Bypass or escape from OIS is thought to be responsible for melanoma tumor development from BRAF-transformed melanocytes. Efforts to validate the OIS model produced conflicting data. While investigations were primarily focused on genetic and epigenetic events within melanocytes, the role skin microenvironment plays in OIS is poorly understood.The overall goal of this project is to understand the role of melanocyte microenvironment in melanoma tumor development. We hypothesize that cellular contact with UV exposed epidermal keratinocytes and/or secreted factors from other skin-resident cells influence OIS-escape and malignant melanoma tumor development. Genetic mouse models and co-culture of isolated human skin cell, although useful, have several limitations. Microfluidic methods offer powerful and versatile alternative to overcome the limitations of these approaches. We will test the hypothesis that skin microenvironment plays a role in melanoma development by employing freshly isolated melanocytes, keratinocytes and fibroblasts on a microfluidic platform.UV-induced changes in miRNA expression and understanding the mechanisms of regulation of miRNAs by UV, therefore, could help early detection, diagnosis and prognosis of malignant melanoma in military personnel. Here, we propose to identify the networks of melanocyte-specific miRNAs and their regulation by exposure to UV that mimics exposure to solar radiation, and investigate the role of this network of miRNAs and their targets in transformation of melanocytes and melanoma development in sun-exposed skin

1. **KEYWORDS:** *Provide a brief list of keywords (limit to 20 words).*

   Melanocytes, malignant transformation, Oncogene-induced senescence, melanomagenesis, skin, microenvironment, keratinocytes, fibroblasts, UV radiation, microfluidics.

2. **ACCOMPLISHMENTS:** *The PI is reminded that the recipient organization is required to obtain prior written approval from the awarding agency Grants Officer whenever there are significant changes in the project or its direction.*

   - **What were the major goals of the project?**

     - Optimize microfluidic methods for enrichment of melanocytes from freshly isolated epidermal cells.
     - Design and optimize microfluidic system to transform melanocytes with BRAF(V600E) and monitor oncogene induced senescence.
     - Test the effect of keratinocytes and fibroblasts on senescence in transformed melanocytes.
     - Identify molecules and mechanism in fibroblast- and UV radiated keratinocyte-mediated effects on oncogene transformed melanocytes.

- **What was accomplished under these goals?**

1) Major activities:

   During this reporting period, we optimized the fabrication of the microfluidic device and patterning melanocytes/ primary melanoma cells and skin keratinocytes and dermal fibroblasts. We standardized methods for secretome analysis and imaging methods. A manuscript describing these results is submitted to the journal Lab on a Chip (a journal of the Royal Society of Chemistry).

2) Specific objectives:

   In this funding period, we proposed the followings tasks:

   Task 1. Optimize melanocyte and keratinocyte isolation-

   Subtask 1a. Optimization of immunocapture using MC1R and cKIT antibodies on the microfluidic device (months 3-4). Partially completed. Delayed to non-availability of fresh skin specimens during the COVID19 restrictions on tissue collection

   Subtask 1b. Lentivirus production and titer using monolayer cells- Completed.

   Subtask 1c. Optimize transduction of melanocytes in the microfluidic chamber- Partially completed. Delayed to non-availability of fresh skin specimens during the COVID19 restrictions on tissue collection

   Task 2. Optimize microfluidic device for melanocyte transformation. In progress

   Subtask 1d. Optimize methods to monitor senescence- In progress

   Task 3. Test the effects of keratinocytes and fibroblasts on OIS in melanocyte.

   Subtask 2a. Optimize isolation of keratinocytes and fibroblasts and seeding in microfluidic device

   Completed.

   Subtask 2b. Cell proliferation, clonogenicity and soft agar assays- To be initiated

3) Significant results:

   Please see the attached manuscript

Microfluidic device and cell confinement

The microfluidic device we fabricated to evaluate the influence of keratinocytes and stromal fibroblasts on primary melanoma cells is shown in Figure 1A. This microdevice has a central circular microchamber to culture melanoma cells with two lateral chambers on the side to seed dermal fibroblasts and/or keratinocytes. The central chamber was connected to the lateral chambers by a series of narrow concentric microchannels of 10μm height. Previous studies have relied on hydrogel patterning in other designs including similar connection microchannels to generate physical barriers or walls. These hydrogels allowed researchers to pattern cells in adjacent chambers while allowing cellular crosstalk. Thus, we treated the microdevices with oxygen plasma to render the material hydrophilic, ensuring that the collagen solution flowed through all the chambers and connection microchannels. Next, we aspirated the collagen solution from the central and lateral chambers, leaving the collagen solution contained inside the connection microchannels. However, our results showed that

hydrogel patterning may be challenging, or even impossible in systems where evaporation occurs rapidly due to the small volume contained in such microchannels (Figure 1B and Supporting movie 1). The time-lapse images showed that the 4mg/ml collagen solution confined in the connection microchannels rapidly evaporated in less than 2 min, making the cell patterning impossible (Supporting Figure 1). In the absence of these hydrogel-walls, cells injected in the lateral chambers immediately flowed through the connecting microchannels and appeared in the central chamber and *vice versa*. Although the microchannel design can be optimized to generate a high fluidic resistance path (e.g., in our design the connection channels had a cross-section 50 times smaller than the central channels, theoretically providing >2000-fold increase in fluidic resistance), cell patterning is extremely challenging without a physical barrier provided by the hydrogel (Supporting Figure 1). Therefore, we explored the use of air-walls to achieve cell confinement without the use of hydrogels or other solutions (Figure 1C). In our PDMS-based microdevice aqueous solutions filled first the fluidic path with the highest cross-section, i.e., the central and lateral chambers, as opposed to the connection channels. A suspension of melanoma cells ($4x10^6$ cells/ml; labelled red) was injected through the central inlet. The cell suspension flowed through the central microchamber and reached the central outlet without entering the connecting microchannels (Figure 1A-E). Next, a second cell suspension containing fibroblasts or keratinocytes ($4x10^6$/ml; labelled green) was perfused through the lateral chamber. These cells reached the lateral outlet without entering the connecting channels. This approach of leveraging the air trapped (air-walls) in the connecting channels allowed us to confine the multiple cell types. After seeding the cells, the microdevices were placed in cell culture incubator at 37ºC and 5% $CO_2$ overnight. Under these conditions the air-walls dissolved in a few hours (Supporting movie 2). Once the air-wall is completely dissolved, liquid occupied the space between the lateral and central chambers, allowing cell migration and cellular crosstalk and (Figure 1F). The time required for the air-walls to dissolve depended on the air-wall volume, providing the flexibility to design air-walls with a different volume to control the dynamics of cell migration and crosstalk (Supporting Figure 3). After 24 hours, fibroblasts and melanoma cells migrated into the connecting channels, reaching the cells located in the adjacent chamber. The use of these air-walls allowed us to pattern melanoma cells, dermal fibroblasts, and epidermal keratinocytes in the central and lateral chambers (Figure 1G). Stromal cell crosstalk induced changes on melanoma cell morphology

Stromal cells such as keratinocytes and dermal fibroblasts surround melanoma cells and have the potential to modify primary tumor evolution and progression. Thus, we co-cultured primary melanoma cells in the presence of dermal fibroblasts and keratinocytes leveraging the air-wall confinement method. Melanoma cells were stained with a red-fluorescent cell tracker and after 3 days in the microdevices, cells were visualized by fluorescence microscopy (Figure 2A). The microscopy images revealed that when cultured in monoculture, melanoma cells formed multicellular clusters with multiple cells grouped together (Figure 2B). On the other hand, when keratinocytes or dermal fibroblasts were present, melanoma cells changed their morphology and transition to a single cell phenotype. The morphological analysis demonstrated that in monoculture, melanoma cells exhibited a circular-like shape (i.e., low aspect ratio), whereas in the presence of dermal fibroblasts or keratinocytes they became more elongated, exhibit a spindle-like morphology (Figure 2C).

Next, we set out to evaluate the molecular crosstalk between dermal fibroblasts, keratinocytes, and melanoma cells. We confined the three cell populations in the microdevice and after 3 days in culture we analyzed secretion of selected chemokines and growth factors (Figure 3A). Presence of fibroblasts, keratinocytes, or both, led to significant changes in chemokine secretion (Figure 3B). More specifically, keratinocytes alone secreted higher levels of IL-6, which were further increased in the triple co-culture with fibroblasts and melanoma cells. IL-6 is a pleiotropic chemokine produced by multiple cell types including melanoma cells and keratinocytes and dermal fibroblasts in response to inflammation or UV exposure. In melanoma, IL-6 has been shown to decrease tumor apoptosis and increase tumor cell proliferation in more advanced stages[25, 26].

Our analysis also revealed increased IL-8 secretion in the context of coexistence of the three cell types. IL-8 has been also associated with increased melanoma invasion, and metastatic potential. Additionally, IL-8 also regulates tumor-induced angiogenesis[27, 28]. Exposure to UV light leads to overexpression of IL-8 in melanoma cells which in turn accelerates tumor growth. In the co-culture conditions, we observed higher amounts of IL-8,

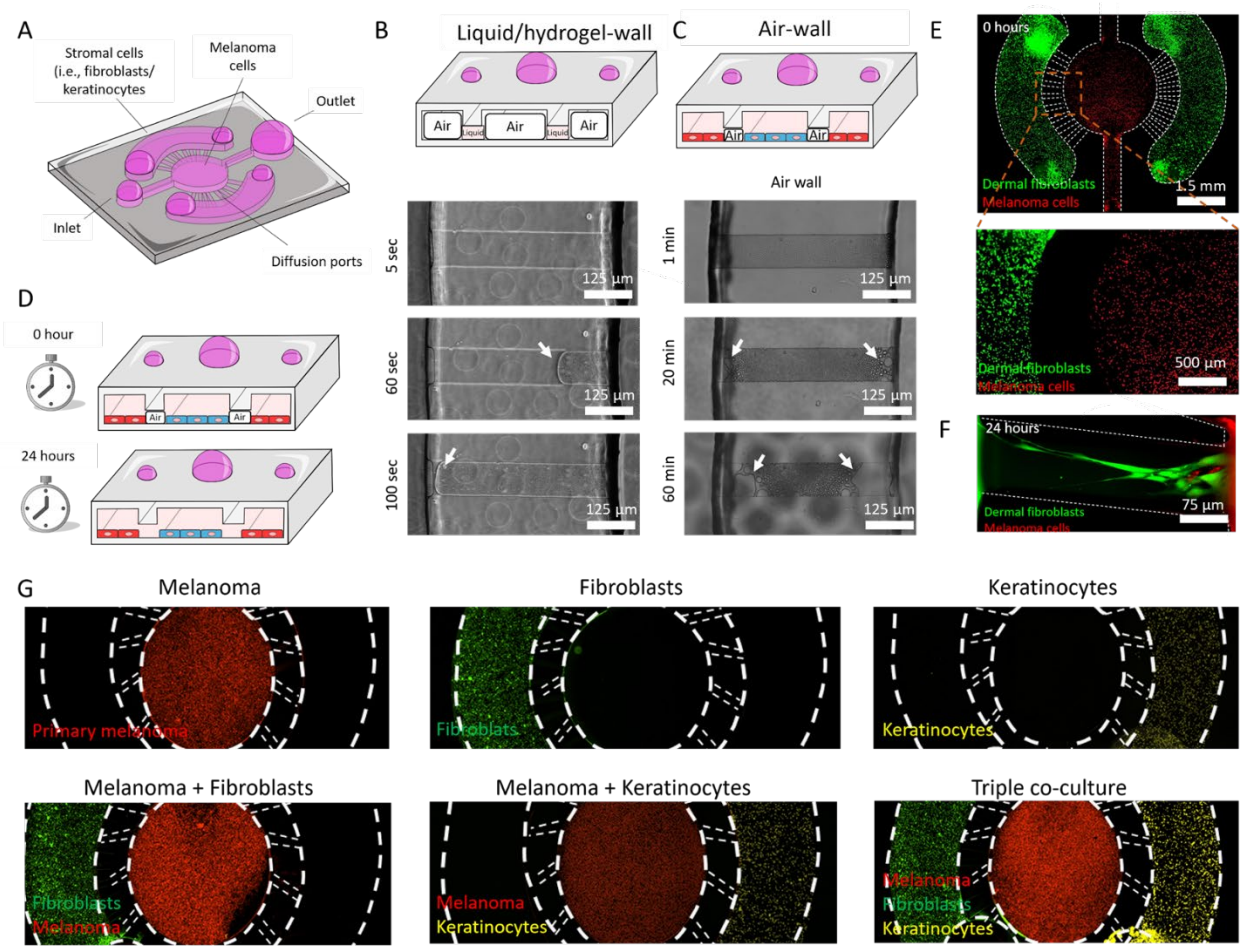


**Figure 1. Microdevice design and air-wall confinement.** A) Scheme depicting the PDMS-based microfluidic device containing the central chamber and two lateral chambers on the sides, connected by a series of concentric narrow microchannels. B) Brightfield time-lapse images showed the evaporation kinetics of liquid-walls. Microdevices were treated with oxygen plasma to render them hydrophilic and ensure the collagen solution flowed through all the chambers and connection microchannels. Next, the collagen solution was aspirated from the lateral and central chambers, leaving the collagen solution confined inside the connection microchannels (upper panel). Given the small volume contained inside the microchannels, the hydrogel solution rapidly evaporated in 2 min (mid- and lower- panel). C and D) Time-lapse images showing the dynamics of the air-wall dissolving. Microdevices were not treated with plasma, to ensure the liquid injected in the lateral and central chambers did not enter the connecting microchannels, generating an air-wall inside these microchannels. The air-wall took several hours to completely dissolve in 10µm-height microchannels, providing the cells enough time to attach to the bottom of the chambers before physically connecting them. E) Melanoma cells and dermal fibroblasts (stained in red and green) were confined in the central and lateral chambers respectively using air-walls. F) After 24 hours, the air-wall was completely dissolved, and cells started to migrate through the connecting microchannels. G) Fluorescence microscopy images showed the confinement achieved by the air-wall method. Melanoma cells, dermal fibroblasts, and keratinocytes were labelled in red, green, and infra-red (shown in yellow) respectively.

but the levels were not significantly higher than the sum of the fibroblasts, keratinocyte, and melanoma mono-culture conditions combined. However, the observations that keratinocytes and dermal fibroblasts secreted IL-8 suggested their tumor-promoting role in melanoma evolution. IL-1β is an immunomodulatory chemokine secreted by multiple immune cells in response to inflammatory signals[29]. In normal conditions, IL-1β contributes to resolving the last steps of the inflammatory response. However, during the chronic inflammation-like environment within the tumor, IL-1β promotes tumor growth and metastasis by multiple mechanisms such as NF-κB, MAPK, AKT, and WNT pathways[29].

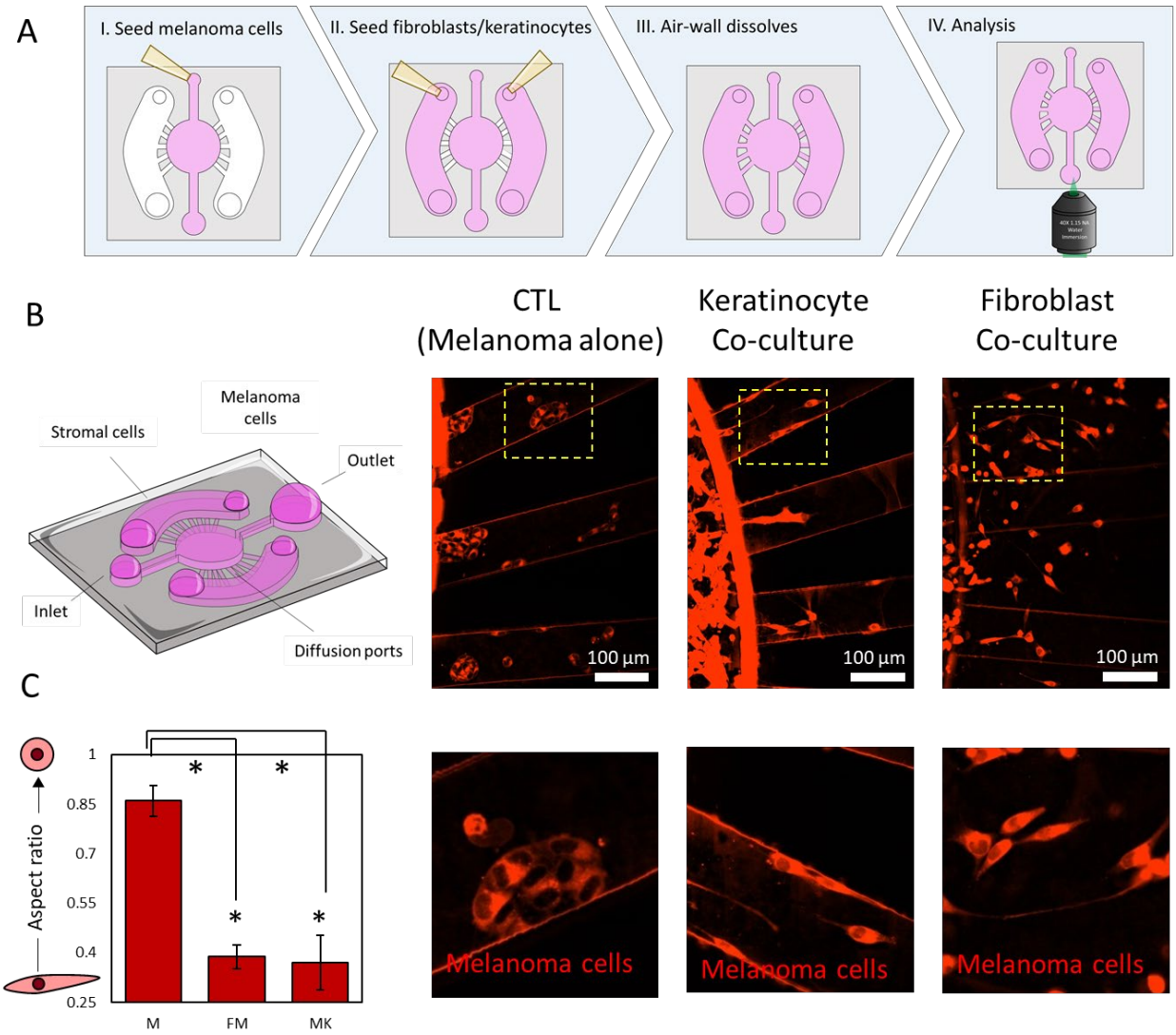


**Figure 2 Morphological analysis.** A) Scheme illustrating the experimental protocol: melanoma cells were confined in the central chamber using the air-wall method with/without dermal fibroblasts/keratinocytes in the lateral chambers. After 3 days in culture, the microdevices were imaged to visualize cell migration and morphology. B) Fluorescence microscopy images showed melanoma cells stained in red after 3 days in culture in monoculture (control condition) and in the presence of fibroblasts, or keratinocytes, or both in the lateral chambers. When cultured alone, melanoma cells formed multicellular clusters. When cultured in the presence of fibroblasts, keratinocytes, or both, melanoma cells spread and appeared as isolated cells. C) Melanoma cell aspect ratio in monoculture and in the presence of dermal fibroblasts and keratinocytes. Asterisks denote p-value<0.05.

Additionally, IL-1β induces the secretion of other chemokines including the IL-1 family which plays a critical role in tumor progression. In this context, we also observed that keratinocytes secreted high levels of IL-1α. Secretion of IL-1α represses the expression of the transcription factor MITF-M, which controls melanocyte differentiation. Accordingly, IL-1α contributes to maintaining undifferentiated state in melanoma cells, which contributes to tumor growth. Additionally, IL-1α decreases the generation of immunogenic antigens, contributing to an immunosuppressive microenvironment within the tumor[30]. Additionally, IL-1α decreases the redox state of melanoma cells and induces the generation of reactive oxygen species (ROS), which in turn also contribute to maintaining a tumor-promoting inflammatory response[29]. These results suggested dermal fibroblasts, and especially keratinocytes, may be playing a tumor-promoting role. However, keratinocytes also secreted IP-10 and MCP-1, which may help to control tumor growth. IP-10 is an angiostatic factor that has

shown a potent antiangiogenic effect[31]. In vivo studies using melanoma models overexpressing IP-10 showed that the tumors had lower microvascular density, slower tumor proliferation and increased apoptosis. However, the exact molecular mechanisms controlling this response remain poorly understood. Recent studies suggested that IP-10-induced angiostatic effects are mediated through the CXCR3 pathway, which has been associated with lymph node metastasis in melanoma[32]. On the other hand, our experiments also revealed that fibroblasts, melanoma cells, and keratinocytes secreted MCP-1, which has been associated with immune regulation[33]. The co-culture of melanoma cells with fibroblasts and/or keratinocytes showed an additive effect rather than synergistic regarding MCP-1 secretion. MCP-1 is a chemoattractant protein that primarily recruits macrophages to the tumor microenvironment[34]. In melanoma, macrophages can play a dual role, promoting or inhibiting tumor growth depending on other co-stimulatory factors present in the surrounding microenvironment. Interestingly, studies have shown that macrophages attracted by MCP-1 can lead to tumor formation in non-tumorigenic lesions[35]. Altogether, our data highlight the complex interactions between primary melanoma cells and skin microenvironment, specifically due to the surrounding keratinocytes and dermal fibroblasts, which can control melanoma transition from localized primary stage to an invasive tumor and metastatic disease. Identification of the key pathways controlling such transitions might lead to new successful therapies to prevent and treat melanoma.

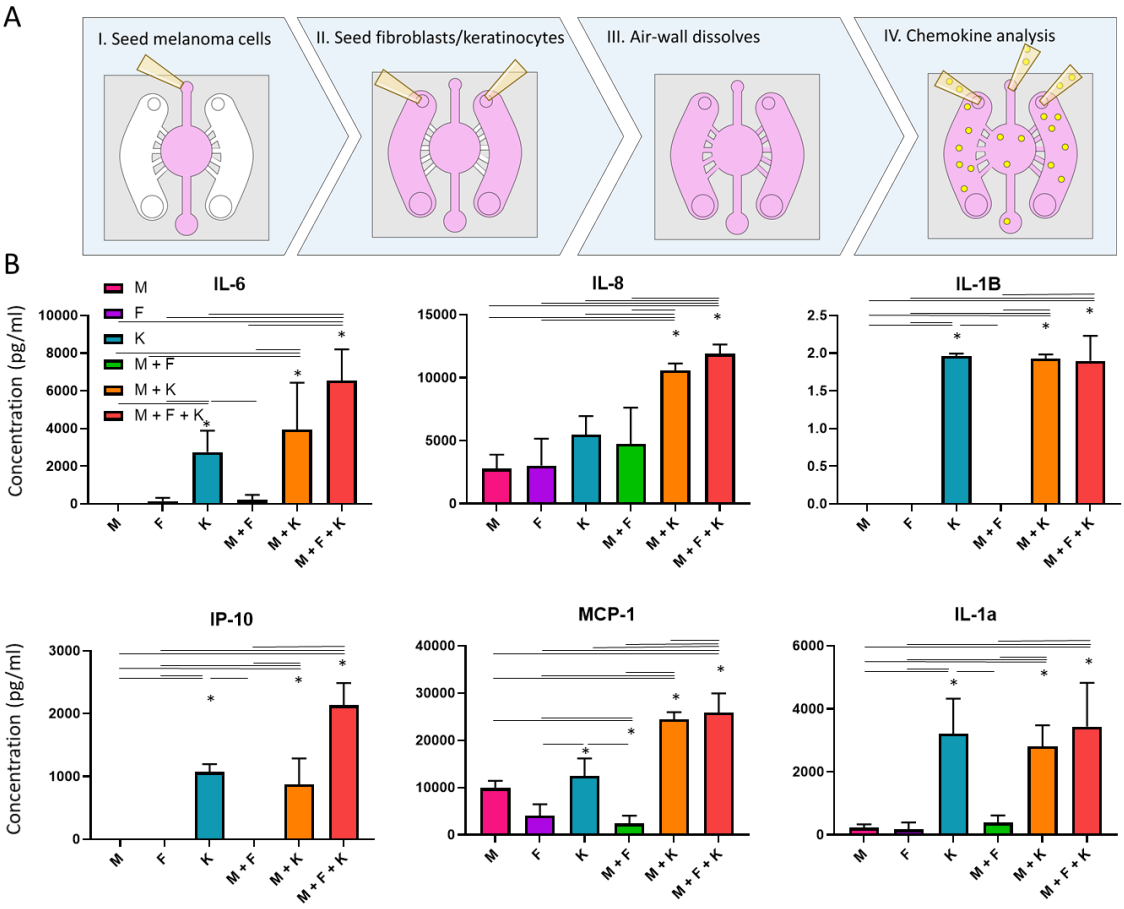


**Figure 3. Cellular crosstalk.** A) Melanoma cells were seeded in the central chamber alone or with dermal fibroblasts and/or keratinocytes on the lateral chambers. After 3days, chemokine secretion was analyzed by MAGPIX. C) Bar graphs showed the chemokine secretion in melanoma cells alone (M), dermal fibroblasts alone (F), keratinocytes alone (K), melanoma with dermal fibroblasts (M + F), melanoma cells and keratinocytes (M + K), and the triple co-culture (M + F + K). Asterisks denote p-value<0.05.

Cell metabolism

Tumor cells exhibit higher proliferation rates compared with normal cells, which forces them to adapt their metabolism to satisfy the high demand of carbohydrates, amino acids, and fatty acids[36]. Altered tumor metabolism offers opportunity to selectively destroy cancer cells without damaging the normal tissue[37]. Therefore, we compared cell metabolism in melanoma cells, dermal fibroblasts, and keratinocytes using optical metabolic imaging (OMI). OMI relies on the use of multi-photon microscopy to visualize the autofluorescence of NAD(P)H and FAD, molecules involved in cell metabolism and cell redox balance (Figure 4A)[38]. Rapidly proliferating cells, such as cancer cells, commonly rely on glycolysis to generate "building blocks" to support cell proliferation, generating an excess of NAD(P)H as a by-product of their anaerobic metabolism[36]. Therefore, we quantified NAD(P)H autofluorescence intensity and divided by the FAD autofluorescence intensity to calculate the normalized redox ratio (Figure 4B and C). The NAD(P)H/FAD ratio has been used in previous studies to monitor cellular redox potential in live cells without any external labeling agent[24, 38, 39]. When cultured alone, melanoma cells exhibited a higher redox ratio compared with dermal fibroblasts and keratinocytes (i.e., normal cells). Interestingly, the co-culture with keratinocytes, dermal fibroblasts, or both, led to a significant change in melanoma cell redox ratio, suggesting a metabolic shift in melanoma cells.

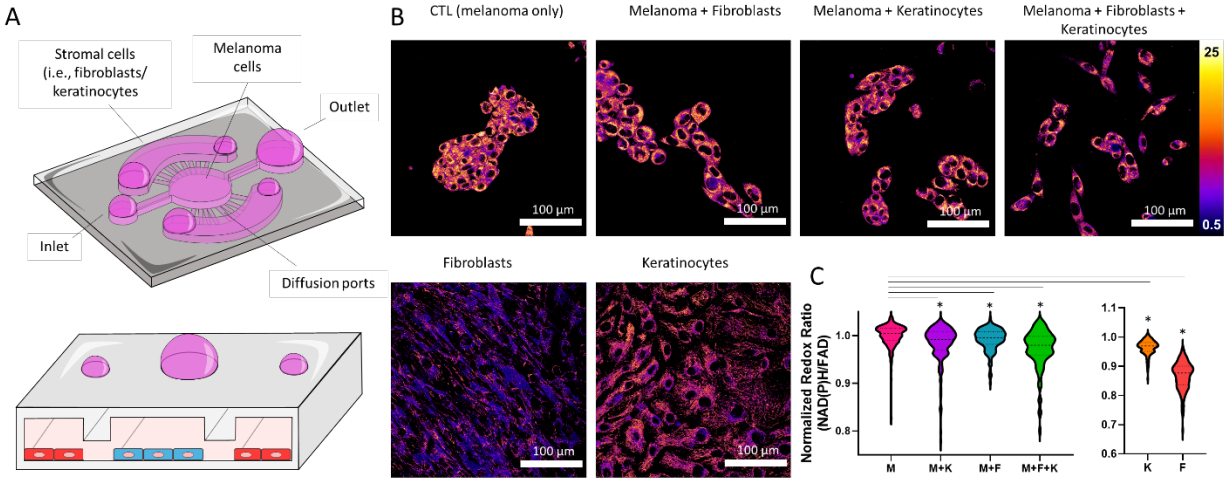


**Figure 4. Optical metabolic imaging.** A) Schematic representation of the triple co-culture inside the microdevice, including melanoma cells, dermal fibroblasts, and keratinocytes. B) Melanoma cells were imaged by multi-photon microscopy. Images shows normalized ratio of NAD(P)H autofluorescence divided by FAD autofluorescence, defined as normalized redox ratio. Melanoma cells were imaged alone and in the presence of dermal fibroblasts and/or keratinocytes. Images of fibroblasts and keratinocytes alone are also shown. C) Right panel shows normalized redox ratio of melanoma cells alone and in the co-culture conditions. Left panel shows normalized redox ratio of dermal fibroblasts and keratinocytes alone. Asterisk denotes a p-value<0.05.

Additionally, we analyzed NAD(P)H fluorescence lifetime (NAD(P)H $\tau_m$) in melanoma cells, dermal fibroblasts, keratinocytes, and multiple combinations (Figure 5). NAD(P)H $\tau_m$ is modulated by the ratio of NAD(P)H free in the cytoplasm to the amount bound to enzymes (e.g., mitochondrial respiratory complexes). Thus, an increase in NAD(P)H $\tau_m$ is associated with an increase in the ratio NAD(P)H-bound vs NAD(PH)-free, which commonly happens during oxidative phosphorylation. Our results demonstrated that melanoma cells had a higher NAD(P)H $\tau_m$ compared with normal cells such as dermal fibroblasts and keratinocytes, demonstrating again the different metabolic phenotype exhibited by melanoma cells. Interestingly, when co-cultured with dermal fibroblasts, keratinocytes, or both, melanoma cells showed a decrease in their NAD(P)H $\tau_m$, which agrees with an increase in the amount of NAD(P)H free in the cytoplasm. These results are consistent with the chemokine analysis (i.e., secretion of tumor-promoting chemokines), suggesting dermal fibroblasts and keratinocytes play a tumor-supporting role. Enabled by this platform, in-depth proteomics, and metabolomics

analysis (e.g., mass spectrometry) could pinpoint the specific molecular alterations driving tumor-stroma crosstalk and melanoma progression.

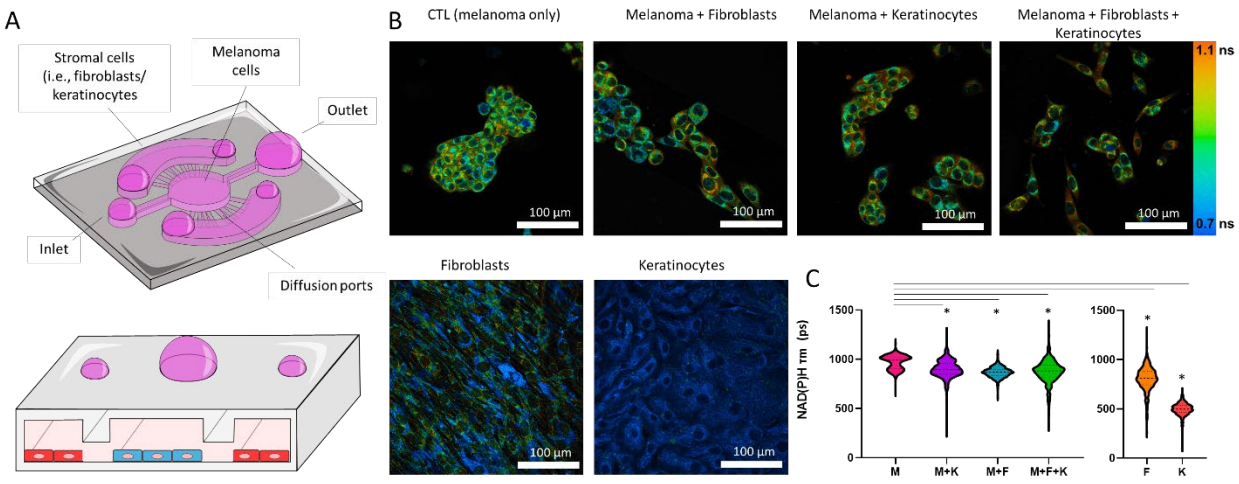


**Figure 5 NAD(P)H FLIM.** A) Schematic representation of the triple co-culture inside the microdevice, including melanoma cells, dermal fibroblasts, and keratinocytes. B) Melanoma cells imaged by multi-photon microscopy. Images show NAD(P)H FLIM. Melanoma cells were imaged alone and in the presence of dermal fibroblasts and/or keratinocytes. Images of fibroblasts and keratinocytes alone are also shown. C) Right panel shows melanoma cell NAD(P)H FLIM alone and in the co-culture conditions. Left panel shows keratinocyte and dermal fibroblast NAD(PH) FLIM. Asterisk denotes a p-value<0.05.

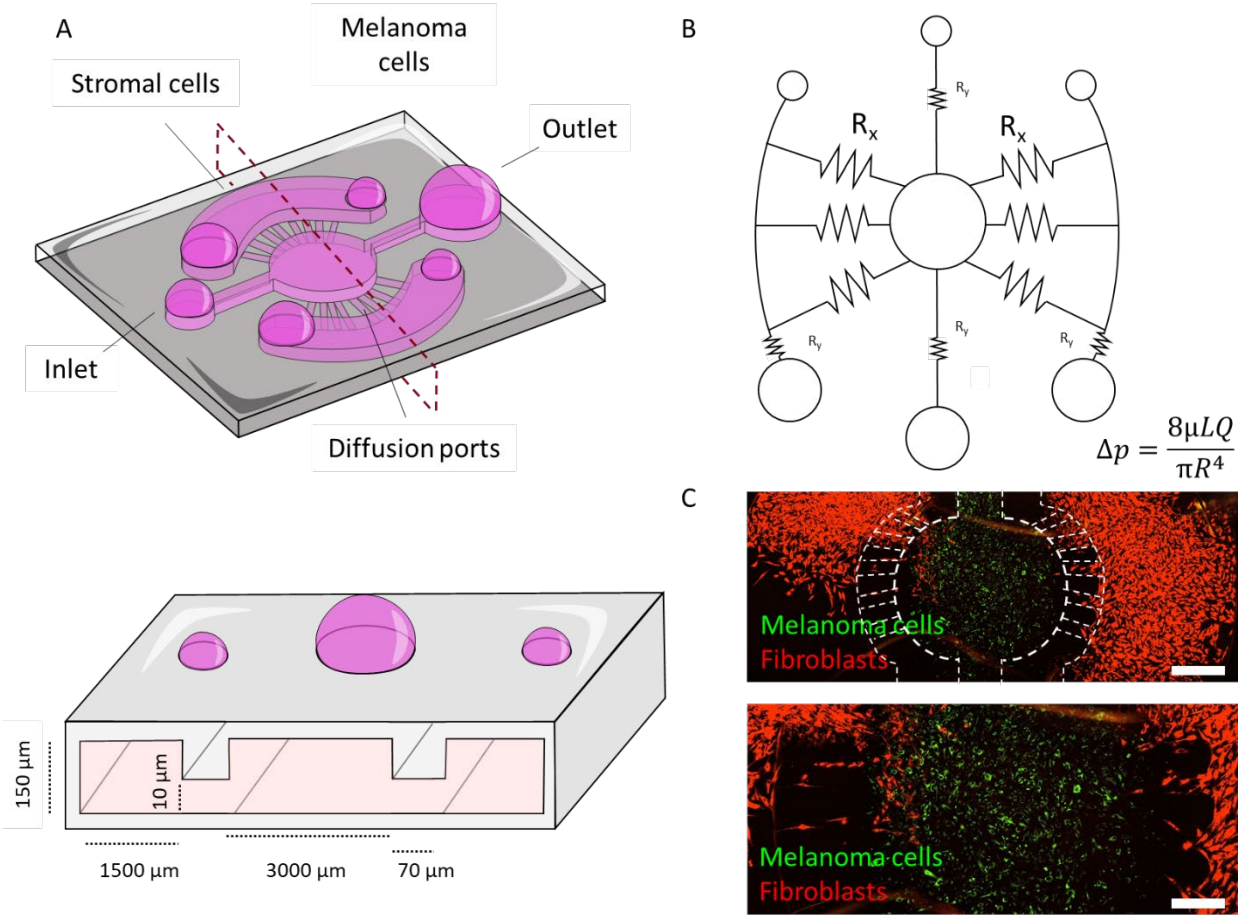


**Supporting Figure 1.** Cell confinement based on fluidic resistance. A) Microdevice scheme. The connection microchannels present a smaller cross-section compared with central channel connecting with the central microchamber. B) Schematic representation of the microdevice demonstrating the difference in fluidic resistance generated by the connection microchannels compared with the path defined by the central chamber and central channel. Bottom right shows the Hagen–Poiseuille equation where Δp is the pressure difference between the two ends, μ is the dynamic viscosity, L is the length of the channel, Q is volumetric flow rate, and R is the radius of the channel. C) Confocal image showing the confinement achieved by fluidic resistance using melanoma cells (in green) and dermal fibroblasts (in red). Fibroblasts can be observed inside the central chamber, demonstrating the presence of crossflow from the lateral chambers towards the central chamber.

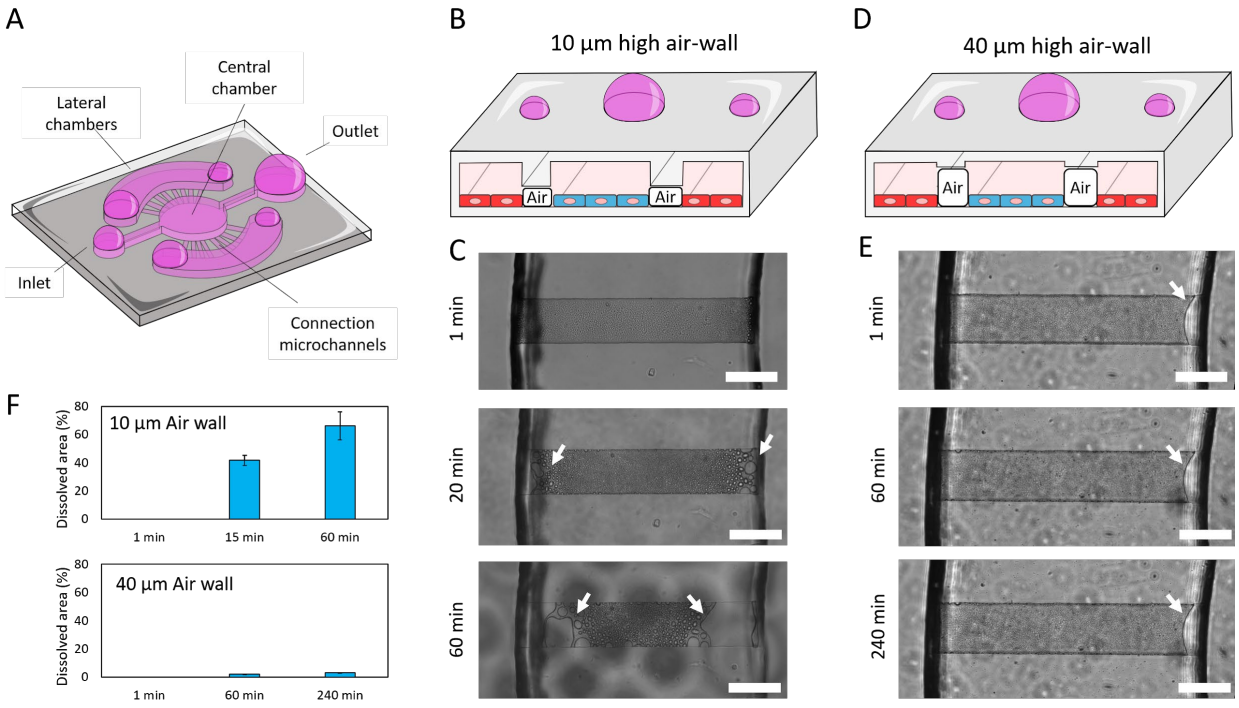


**Supporting Figure 2 Effect of air volume on the air-wall dynamics.** A) Scheme of the microdevice design. B) Schematic representation of a microdevice designed with 10µm-height connection microchannels. C) 60 minutes time-lapse images showing the air-wall dissolving. After 60 minutes, 65% of the air-wall appeared to be dissolved, observing droplets of different sizes (white arrows). D) Schematic representation of a microdevice designed with 40µm-height connection microchannels. E) 240 minutes time-lapse images showing less than 5% of the air-wall dissolving. F) Bar graph showed the percentage of air-wall dissolved at different time-points in the 10 and 40µm-height air-wall microdevices. The results demonstrate the effect of the air-wall height in the dissolving dynamics.

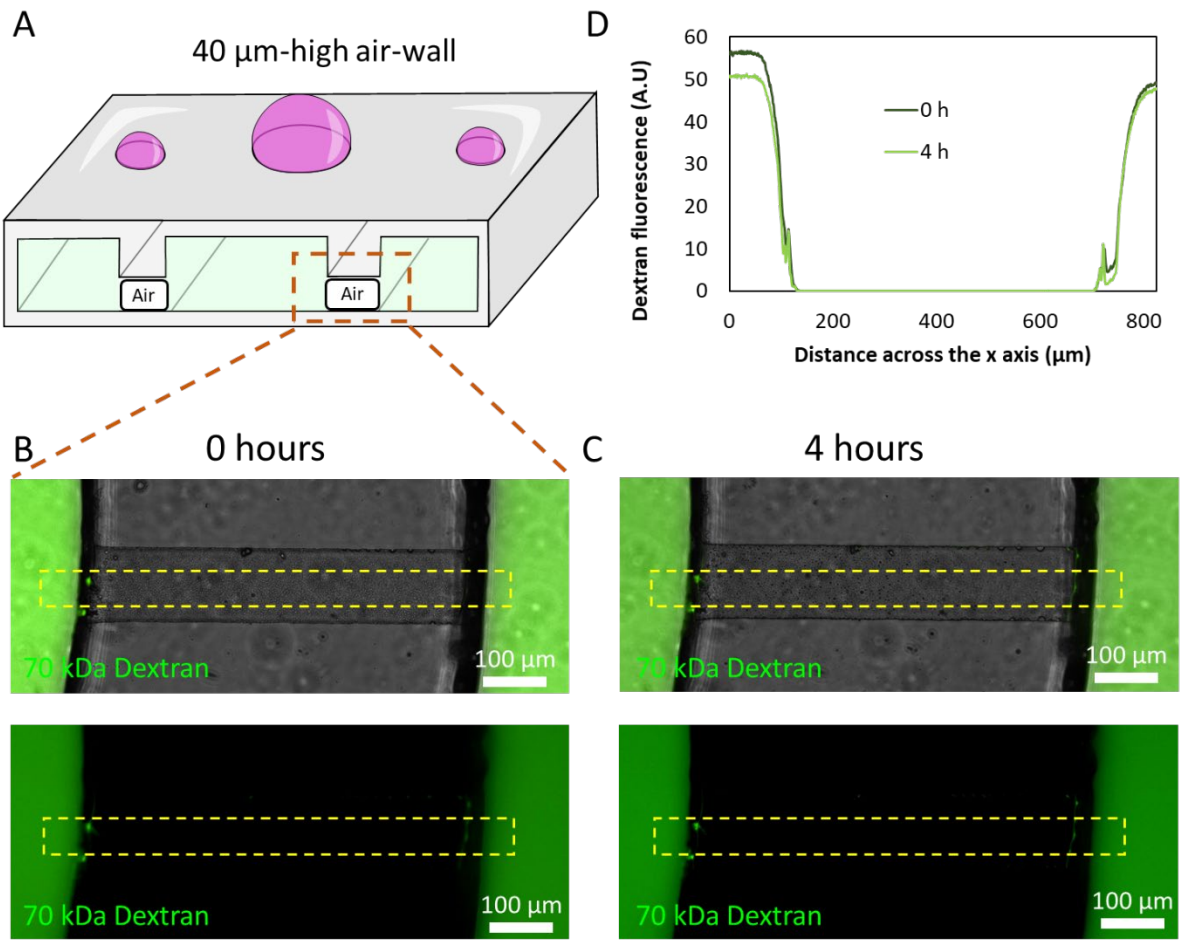


**Supporting Figure 3. Air-walls prevent molecular diffusion.** A) Schematic showing a 40µm-high air-wall separating a 10µM fluorescent 70kDa-dextran solution. The dextran solution was perfused in the central and lateral chambers, generating an air-wall in the connection channel. B-C) Fluorescence microscopy images showing dextran fluorescence at 0 and 4 hours post-dextran injection. D) Graph analyzed the fluorescent profile across the delimited region in B and C (i.e., yellow rectangle). The profile showed no dextran diffusion across the connection channel after 4 hours in culture.

- **What do you plan to do during the next reporting period to accomplish the goals?**
    - We will complete the tasks initiated during this reporting period- specifically isolation and enrichment of fresh melanocytes, and trasnsformation of melanocytes in the microdevice for Task 2
    - Optimize UV exposure of keratinocytes and seeding in the microdevice
    - Complete the study on the effect of keratinocytes and fibroblasts on melanocyte senescence, proliferation and clonogenicity.
    - Complete proteomic/secretome analysis.
    - Isolate RNA and submit for RNA-Seq and analyze data

3. **IMPACT:** *Describe distinctive contributions, major accomplishments, innovations, successes, or any change in practice or behavior that has come about as a result of the project relative to:*
    - **What was the impact on the development of the principal discipline(s) of the project?**
        - The microfluidic device developed here is novel and its application to understanding the role of skin microenvironment on melanocyte transformation has the potential to improve our understanding of melanoma tumor initiation and progression.
    - **What was the impact on other disciplines?**
        - While tumor cell intrinsic (genetic and epigenetic) factors have received much attention in understanding cancer initiation and progression, the role of tissue microenvironment on this process is not well understood. This strategy described here could be adapted to understand initiation of other cancers.
    - **What was the impact on technology transfer?**
        - Nothing to Report
    - **What was the impact on society beyond science and technology?**
        - Nothing to Report for this period
4. **CHANGES/PROBLEMS:** *The Project Director/Principal Investigator (PD/PI) is reminded that the recipient organization is required to obtain prior written approval from the awarding agency Grants Officer whenever there are significant changes in the project or its direction. If not previously reported in writing, provide the following additional information or state, "Nothing to Report," if applicable:*
    - **Changes in approach and reasons for change**
        - Nothing to Report.
    - **Actual or anticipated problems or delays and actions or plans to resolve them**
        - Due to restrictions on collecting skin specimens from the hospital during the COVID19, experiments requiring freshly isolated skin cells have been delayed. The request for

resumption of skin collection is currently being reviewed for approval. If we do not obtain a timely approval to continue the experiments, we may consider using existing melanocytes, keratinocytes and fibroblasts (all at passage 1 or 2).

- **Changes that had a significant impact on expenditures**
  - Due to research shut down at University of Wisconsin-Madison between March 16-June 1, there were no expenditures for supplies.
- **Significant changes in use or care of human subjects, vertebrate animals, biohazards, and/or select agents**
  - Nothing to Report.

5. **PRODUCTS:** *List any products resulting from the project during the reporting period. If there is nothing to report under a particular item, state "Nothing to Report."*
   - **Publications, conference papers, and presentations**
     *Report only the major publication(s) resulting from the work under this award.*
     - **Journal publications.**
       - Submitted. Please see the attached.
     - **Books or other non-periodical, one-time publications.**
       - Nothing to report.
     - **Other publications, conference papers, and presentations.**
       - Nothing report.
   - **Website(s) or other Internet site(s)**.
     - Nothing to report
   - **Technologies or techniques.**
     - Nothing to report.
   - **Inventions, patent applications, and/or licenses**
     - Nothing to report.
   - **Other Products**
     - Nothing to report.
6. **PARTICIPANTS & OTHER COLLABORATING ORGANIZATIONS**
   - **What individuals have worked on the project?**
     -

| Name | Project Role | Researcher ID | Nearest person month worked | Contribution to Project | Funding Support |
|---|---|---|---|---|---|
| Setaluri, Vijaysaradhi | Principal Inv. | N/A | 1.2 | Design and analysis | N/A |
| Jose Maria Ayuso | Postdoc. | N/A | 9.6 | Microfluidic device design, and all experiments | N/A |
| Shreyans Sadangi | Res. Asst. | N/A | 12 | Performed all cell culture experiments | N/A |

   - **Has there been a change in the active other support of the PD/PI(s) or senior/key personnel since the last reporting period?**
     - Nothing to report
   - **What other organizations were involved as partners?**
     - NOT APPLICABLE/Nothing to report

- *Describe partner organizations - academic institutions, other nonprofits, industrial or commercial firms, state or local governments, schools or school systems, or other organizations (foreign or domestic) - that were involved with the project. Partner organizations may have provided financial or in-kind support, supplied facilities or equipment, collaborated in the research, exchanged personnel, or otherwise contributed. Provide the following information for each partnership:*
    - **Organization Name:**
    - **Location of Organization:** *(if foreign location list country)*
    - **Partner's contribution to the projec**t *(identify one or more)*
        - **Financial support;**
        - **In-kind support** *(e.g., partner makes software, computers, equipment, etc., available to project staff)*;
        - **Facilities** *(e.g., project staff use the partner's facilities for project activities)*;
        - **Collaboration** *(e.g., partner's staff work with project staff on the project)*;
        - **Personnel exchanges** *(e.g., project staff and/or partner's staff use each other's facilities, work at each other's site)*; and
        - **Other.**

7. **SPECIAL REPORTING REQUIREMENTS** - NONE
    - **COLLABORATIVE AWARDS:** *For collaborative awards, independent reports are required from BOTH the Initiating PI and the Collaborating/Partnering PI. A duplicative report is acceptable; however, tasks shall be clearly marked with the responsible PI and research site. A report shall be submitted to https://ers.amedd.army.mil for each unique award.*
    - **QUAD CHARTS:** *If applicable, the Quad Chart (available on https://www.usamraa.army.mil) should be updated and submitted with attachments.*
8. **APPENDICES:** *Attach all appendices that contain information that supplements, clarifies or supports the text. Examples include original copies of journal articles, reprints of manuscripts and abstracts, a curriculum vitae, patent applications, study questionnaires, and surveys, etc.*

    Manuscript submitted to Lab on Chip

**APPENDIX**

# A microfluidic device with air-walls to study the effect of skin microenvironment on primary melanoma cells

Jose M Ayuso[1], Shreyans Sadangi[2], Marcos Lares[2], Shujah Rehman[3,4,5], Mouhita Humayun[1], Kathryn M Denecke[1], Melissa C Skala[3,4,5], David J Beebe[1,4,5], Vijayasaradhi Setaluri[2,6].

[1]Department of Pathology & Laboratory Medicine, [2]Dermatology and [3]Biomedical Engineering, University of Wisconsin-Madison, Madison, WI, USA; [4]Morgridge Institute for Research, Madison, WI, USA; [5]UW Carbone Comprehensive Cancer Center, Madison, WI and [6]William S. Middleton VA Hospital, Madison, WI, USA.

Address all correspondence to:

Vijayasaradhi Setaluri, PhD
Professor, Department of Dermatology
Wisconsin Institutes for Medical Research
1111 Highland Ave, Madison, WI 53705 USA

Jose Maria Ayuso, PhD
Postdoctoral fellow
Wisconsin Institutes for Medical Research
1111 Highland Ave, Madison, WI 53705 USA

**Abstract**

Primary melanoma evolution is a complex process where dermal fibroblast and keratinocytes modulate tumor behavior. However, the mechanisms behind these tumor-stroma interactions remain poorly understood. Here, we used a microfluidic platform to evaluate the cross-talk between human primary melanoma cells, dermal fibroblasts, and keratinocytes. The microfluidic device included multiple circular chambers separated by a series of narrow connection channels. The microdevice design allowed us to develop a new cell patterning method based on air-walls, removing the need for hydrogel barriers, porous membranes, or external equipment. Using this method, we co-cultured melanoma cells in the presence of dermal fibroblasts and keratinocytes. The results demonstrated that the presence of dermal fibroblasts and keratinocytes led to changes in melanoma cell morphology and growth pattern. Molecular analysis revealed changes in the chemokine secretion pattern, identifying multiple compounds involved in tumor progression. Finally, optical metabolic imaging showed melanoma cells, fibroblasts, and keratinocytes exhibited a different metabolic signature. Additionally, the presence of stromal cells led to a metabolic shift in melanoma cells, highlighting the role of stromal cells on melanoma evolution.

## Introduction

Cutaneous melanoma is one of the most common malignancies in the U.S. and western countries[1]. Additionally, melanoma incidence has more than tripled in the last decades (1975-2020). American Cancer Society estimates that more than one hundred thousand new melanoma cases will be diagnosed, with nearly eight thousand deaths during 2020 in the US[2]. Melanoma is caused by malignant transformation of melanocytes (i.e., pigment-producing cells located in the skin) that acquire capacity for unregulated proliferation, initially in the skin[3]. Once melanoma cells leave the epidermis (i.e. the most superficial layer of the skin) and enter the underlying tissue layers (e.g., the dermis and the submucosa), the tumor has become invasive, which increases the risk of metastasis and worsens the patient's prognosis[4]. While most studies on melanoma progression focused on molecular changes that occur in primary melanoma cells, the role of skin microenvironment, specifically crosstalk between melanoma cells and epidermal keratinocytes and dermal fibroblasts (the major cell types in the skin), in driving melanoma progression and metastasis are still poorly understood. In this context, the ability of melanocytes to invade the dermis alone is not a malignant feature by itself, as some “nevi” (e.g., moles or birthmarks) are also associated with benign melanocytes in the dermis that do not lead to melanoma[5].

Previous studies have shown that melanoma cell invasion is a complex process where the interactions between the cancer cells and stromal cells (e.g., dermal fibroblasts and keratinocytes) play a critical role[6-8]. Skin fibroblasts and keratinocytes, and melanoma cells secrete multiple growth factors and cytokines that affect numerous cellular functions such as cell migration, proliferation, and metabolism[7]. In addition, tumor-stroma crosstalk has also been shown to modulate treatment response (e.g., stromal cells induce resistance to BRAF inhibitors)[9]. Thus, understanding the cell crosstalk between melanoma cells and stromal cells could be critical for the identification of predictors of melanoma progression, and for the development of successful therapies.

Microfluidic devices allow control of cell location and patterning, making them versatile tools to study cellular crosstalk[10-14]. Previous microfluidic devices relied on porous membranes to separate multiple microfluidic chambers and generate patterned co-cultures[11, 15-17]. Depending on the membrane properties and pore size, these membranes can block the cell diffusion during the seeding process, while they allow secreted chemokines and other signaling factors to diffuse through the membrane pores. Other microdevices have employed hydrogels to generate patterned co-cultures[13, 18-20]. In these systems, a solution of collagen, fibrinogen or other

extracellular matrix protein, is introduced through a microfluidic channel that is flanked by two or more lateral chambers. The hydrogel provides a physical barrier and allows seeding one cell type on each side of the hydrogel barrier. This method has been used to study cell crosstalk in tumor-induced angiogenesis[21], chemotaxis[13] and immune cell infiltration[22]. However, the presence of the hydrogel also poses some limitations: 1) some cell types might not be able to migrate through the hydrogel (e.g., fibrin hydrogels are difficult to degrade for multiple cell types); 2) hydrogels can bind secreted proteins such as chemokines and growth factors, hindering or biasing cellular crosstalk; 3) hydrogels are prone to evaporation, limiting their use when the volume of hydrogel is limited. In this study, we have leveraged a new cell patterning method based on the use of air-walls to study cellular crosstalk. We fabricated a microfluidic device with a central chamber flanked by two lateral chambers on the sides, connected by a series of narrow microchannels. We used air-walls to pattern cutaneous primary melanoma cells, dermal fibroblasts, and epidermal keratinocytes in the multiple chambers of the microdevice. After these air-walls were resolved, we studied the effects of fibroblasts and keratinocytes on morphology of melanoma cells, chemokine secretion and cellular metabolism.

## Materials and Methods

### Microdevice Fabrication

The first step to fabricate any microdevice is to get the SU-8 design of choice on the Silicon wafer. This is done by using a complementary photomask which only exposes the area of choice in the SU-8 and lets that polymerize. Upon the wafer, liquid PDMS is poured and polymerized. Solid PDMS is then peeled off and plasma bonded to a petri dish. The design for this experiment involves a central chamber and 2 lateral chambers, each with a loading port.

Details of the microdevice fabrication are described previously[23]. Two templates, top and bottom, were generated using Illustrator and fabricated with SU-8 lithography techniques. Upon completion, this template was used to generate the microdevices. PDMS was poured on both the top and bottom template and a minimum of 30lbs was placed on the templates as it polymerized for 4 hours at 80 °C. The devices were peeled off the wafer and additional polymerized PDMS covering the ports was removed. Then the PDMS was placed in an isopropyl solution for 10 minutes, after the two sides were placed together creating a cavity. A 340μm-diameter PDMS rod was inserted. Then the device underwent plasma bonding to a 60mm glass-bottom Petri dish. Before use in cell culture, the devices were sterilized with 15 minutes of UV exposure. Finally, the microdevices were treated with polyethyleneimine (Sigma-Aldrich, 03880) diluted in water at 2%

for 10 minutes and then treated with glutaraldehyde (Sigma-Aldrich, G6257) diluted at 0.4% in water for 30 minutes.

Cell isolation

Primary dermal fibroblasts and keratinocytes were isolated from fresh neonatal foreskin specimens in the Cell Culture Core of UW Skin Disease Research Center. Specimens are collected in 10mL DMEM (Gibco) with 1% antibiotics/antimycotics (Gibco) and 2% FBS (Corning) and stored at 4C until processing begins (within 24 hours of collection). After collecting the samples, tissue specimens were placed in 10cm-dishes and washed three times with 4oC HBSS (Hyclone) supplemented with 1% antibiotics/antimycotics to remove residual blood from the circumcision process. Excess fat and connective tissue were removed with curved surgical scissors, placed in a new 10cm-dish, and rinsed five times with 4°C antibiotic-supplemented HBSS. After the 5th wash, the specimen was cut into 4x4mm pieces with a scalpel blade and stored in a 10cm-dish containing 0.5% trypsin-EDTA 10X (Fisher Scientific) with the most superficial layer of skin, or epidermis, facing up for 16-24h at 4°C. After trypsin digestion, the small pieces of tissue were transferred into a 6cm-dish containing supplemented HBSS with 10% FBS to inactivate trypsin. The epidermis containing keratinocytes was then removed from the dermis using forceps and remained in supplemented HBSS solution. Keratinocytes were released from the epidermal sheet by vigorous pipetting. The epidermal sheet and cell suspension were filtered through a 70μm cell strainer to remove tissue debris and washed with 5mL supplemented HBSS solution and collected in a 50mL conical tube. The volume of the collected cell suspension was pipetted into a 15mL conical tube and centrifuged at 1200rpm for 5 minutes to pellet the cells. After supernatant is discarded, keratinocyte specific media was used to resuspend the cells (i.e., 154 media (Gibco) containing Human Keratinocyte Growth Medium (Gibco) and 1% penicillin/streptomycin (Gibco), and the cell suspension was plated in a 6 well plate and incubated at 37C and 5% CO2. Media is changed 24 hours after initial plating and every other day until cultures reach 70% confluency. Fibroblasts were dissociated from the dermal tissue by placing the dermis pieces in a 50mL conical tube containing dispase/collagenase solution (1mg/mL) and incubated at 37C and 5% CO2 for two hours. DMEM containing 10% FBS was then added to inactivate the enzyme solution. Dermal tissue and cell suspension were vigorously pipetted to release fibroblasts, filtered through a 70m cell strainer and collected in a 50mL conical tube. The cell strainer was washed with 4°C antibiotic supplemented HBSS solution. The cell suspension was centrifuged at 1200rpm for 5 minutes and the cell pellet was resuspended in DMEM +10%

FBS +1% pen/strep, plated in a 6 well plate and incubated at 37C and 5% CO2. Media is changed 24 hours after initial plating and every other day until cultures reach 70% confluency.

Cell Culture

Metastasis-competent cutaneous primary melanoma cell line WM-115 was obtained from Rockland Immunochemicals (Limerick, PA). The cell line was established from a 55-year old female melanoma patient and harbors oncogenic mutation BRAFV600D and hemizygous deletion of tumor suppressor PTEN. Melanoma cells were cultured in Tumor Specialized Media containing 10% FBS and Pen/Strep.

Cell staining and fluorescence microscopy

Melanoma cells, keratinocytes, and dermal fibroblasts were stained, respectively, with Cell Tracker Red (10μM, C34552), Calcein AM (green) (10μM; C1430) and Vybrant (infrared) (20μM; DiD V22887, Thermo Fisher) to monitor cell confinement and migration in the microdevice. Cells were trypsinized and stained with the respective stain for 5 min. Next, cells were centrifuged and washed twice with 15 ml of PBS to remove the excess of staining. After seeding the cells in the microdevice, cell confinement, migration and morphology were analyzed in a Niken TiE with temperature and $CO_2$ control system set at 37$^{o}$C and 5% respectively.

Multiplexed assay for measurement of cytokine secretions

To measure cytokines secreted in the media of monoculture and co-culture systems, a multiplexed bead-based assay was used. Media was collected after 48 and 72 hours in culture and samples were prepared and analyzed using the Inflammation 20-Plex Human ProcartaPlex™ Panel (EPX200-12185-901, Thermo Fisher) following the manufacturer's guidelines. Briefly, cytokines were detected by sequentially incubating with antibody bead cocktail solution, detection antibody and streptavidin-R-phycoerythrin. Magnetic beads were washed using a magnetic plate washer prior to mixing with samples and after each incubation. Samples were read on MAGPIX Luminex Xmap system (Luminex Corporation, Austin, Texas) using Luminex xPonent software. The results were expressed as mean fluorescence intensity (MFI) for each analyte in each sample. MFI values from standards were converted to concentrations (pg/mL) using cytokine-specific standard curve data.

Optical metabolic imaging

A custom-built inverted multiphoton microscope (Bruker Fluorescence Microscopy, Middleton, WI) was used to acquire fluorescence intensity and lifetime images. The equipment consists of an ultrafast laser (Spectra Physics, Insight DSDual), an inverted microscope (Nikon, Eclipse Ti), and a 40× water immersion (1.15NA, Nikon) objective. Next, NAD(P)H and FAD images were obtained for the same field of view. FAD fluorescence was isolated using an emission bandpass filter of 550/100 nm and excitation wavelength of 890 nm. NAD(P)H fluorescence was isolated using an emission bandpass filter of 440/80 nm and an excitation wavelength of 750 nm. Subsequently, fluorescence lifetime images were collected using time-correlated single-photon counting electronics (SPC-150, Becker and Hickl) and a GaAsP photomultiplier tube (H7422P-40, Hamamatsu). 512-pixel images were obtained using a pixel dwell time of 4.8 µs over 60s total integration time. To acquire adequate photon observations for lifetime decay with no photobleaching, the photon count rates were maintained at 1–2 × $10^5$ photons/s. The instrument response function was calculated from the second harmonic generation of urea crystals excited at 900 nm, and the full width at half maximum (FWHM) was measured to be 244 ps. A Fluoresbrite YG microsphere (Polysciences Inc.) was imaged as a daily standard for fluorescence lifetime. The lifetime decay curves were fit to a single exponential decay and the fluorescence lifetime was measured to be 2.1 ns (n=7), which is consistent with published values.

Image analysis

NAD(P)H and FAD intensity and lifetime images were analyzed using SPCImage software (Becker & Hickl) as described previously in [24]. The fluorescence lifetime decay curve was deconvolved with the instrument response function and fit to a two-component exponential decay model at each pixel, $I(t)=\alpha1*e(-t/\tau1)+\alpha2*e(-t/\tau2) + C$, where I(t) represents the fluorescence intensity at time t after the laser excitation pulse, α accounts for the fractional contribution from each component, C represents the background light, and τ is the fluorescence lifetime of each component. Since both NAD(P)H and FAD can exist in two conformational states, bound, or unbound to enzymes, a two-component model was used. The short and long lifetime components reflect the bound and unbound conformations, respectively for FAD. While the opposite is true for NAD(P)H, the short and long lifetime components correspond with the unbound and bound conformations, respectively. The mean lifetime (τm) was calculated using, $\tau m = \alpha1\tau1+ \alpha2\tau2$ for both NAD(P)H and FAD. The optical redox ratio was determined from the NAD(P)H and FAD lifetime data by integrating the photons detected at each pixel in the image to calculate the total

intensity. For each pixel, the intensity of NAD(P)H was then divided by the intensity of FAD. Using Cell Profiler, an automated cell segmentation pipeline was created. This system identified pixels belonging to nuclear regions by using a customized threshold code. Cells were recognized by propagating out from the nuclei within the image. To refine the propagation and to prevent it from continuing into background pixels, an Otsu Global threshold was used. The cell cytoplasm was defined as the cell borders minus the nucleus. Values for NADH τm, FAD τm, NAD(P)H intensity, FAD intensity, and the optical redox ratio (NAD(P)H/FAD intensity) were averaged for all pixels within each cell cytoplasm. At least 100 cells per sample were analyzed, and every experiment was repeated at least three times. Confocal microscopy images were analyzed by FIJI (NIH, https://imagej.net/Fiji). To examine molecule diffusion and cell viability, a rectangle-shape region was drawn, and the intensity profile was calculated using FIJI software.

### Statistical analysis

The normal distribution assumption for statistical tests was confirmed by the Kolmogorov-Smirnov test. Statistical significance was set at $p < 0.05$. For nonparametric comparisons, a Kruskal-Wallis test was performed followed by the Mann-Whitney U test. Analysis was performed in GraphPah Prism 8 (https://www.graphpad.com/scientific-software/prism/).

## Results and discussion

### Microfluidic device and cell confinement

The microfluidic device we fabricated to evaluate the influence of keratinocytes and stromal fibroblasts on primary melanoma cells is shown in Figure 1A. This microdevice has a central circular microchamber to culture melanoma cells with two lateral chambers on the side to seed dermal fibroblasts and/or keratinocytes. The central chamber was connected to the lateral chambers by a series of narrow concentric microchannels of 10μm height. Previous studies have relied on hydrogel patterning in other designs including similar connection microchannels to generate physical barriers or walls. These hydrogels allowed researchers to pattern cells in adjacent chambers while allowing cellular crosstalk. Thus, we treated the microdevices with oxygen plasma to render the material hydrophilic, ensuring that the collagen solution flowed through all the chambers and connection microchannels. Next, we aspirated the collagen solution from the central and lateral chambers, leaving the collagen solution contained inside the

connection microchannels. However, our results showed that hydrogel patterning may be challenging, or even impossible in systems where evaporation occurs rapidly due to the small volume contained in such microchannels (Figure 1B and Supporting movie 1). The time-lapse images showed that the 4mg/ml collagen solution confined in the connection microchannels rapidly evaporated in less than 2 min, making the cell patterning impossible (Supporting Figure 1). In the absence of these hydrogel-walls, cells injected in the lateral chambers immediately flowed through the connecting microchannels and appeared in the central chamber and *vice versa*. Although the microchannel design can be optimized to generate a high fluidic resistance path (e.g., in our design the connection channels had a cross-section 50 times smaller than the central channels, theoretically providing >2000-fold increase in fluidic resistance), cell patterning is extremely challenging without a physical barrier provided by the hydrogel (Supporting Figure 1). Therefore, we explored the use of air-walls to achieve cell confinement without the use of hydrogels or other solutions (Figure 1C). In our PDMS-based microdevice aqueous solutions filled first the fluidic path with the highest cross-section, i.e., the central and lateral chambers, as opposed to the connection channels. A suspension of melanoma cells ($4x10^6$ cells/ml; labelled red) was injected through the central inlet. The cell suspension flowed through the central microchamber and reached the central outlet without entering the connecting microchannels (Figure 1A-E). Next, a second cell suspension containing fibroblasts or keratinocytes ($4x10^6$/ml; labelled green) was perfused through the lateral chamber. These cells reached the lateral outlet without entering the connecting channels. This approach of leveraging the air trapped (air-walls) in the connecting channels allowed us to confine the multiple cell types. After seeding the cells, the microdevices were placed in cell culture incubator at 37ºC and 5% $CO_2$ overnight. Under these conditions the air-walls dissolved in a few hours (Supporting movie 2). Once the air-wall is completely dissolved, liquid occupied the space between the lateral and central chambers, allowing cell migration and cellular crosstalk and (Figure 1F). The time required for the air-walls to dissolve depended on the air-wall volume, providing the flexibility to design air-walls with a different volume to control the dynamics of cell migration and crosstalk (Supporting Figure 3). After 24 hours, fibroblasts and melanoma cells migrated into the connecting channels, reaching the cells located in the adjacent chamber. The use of these air-walls allowed us to pattern melanoma cells, dermal fibroblasts, and epidermal keratinocytes in the central and lateral chambers (Figure 1G).

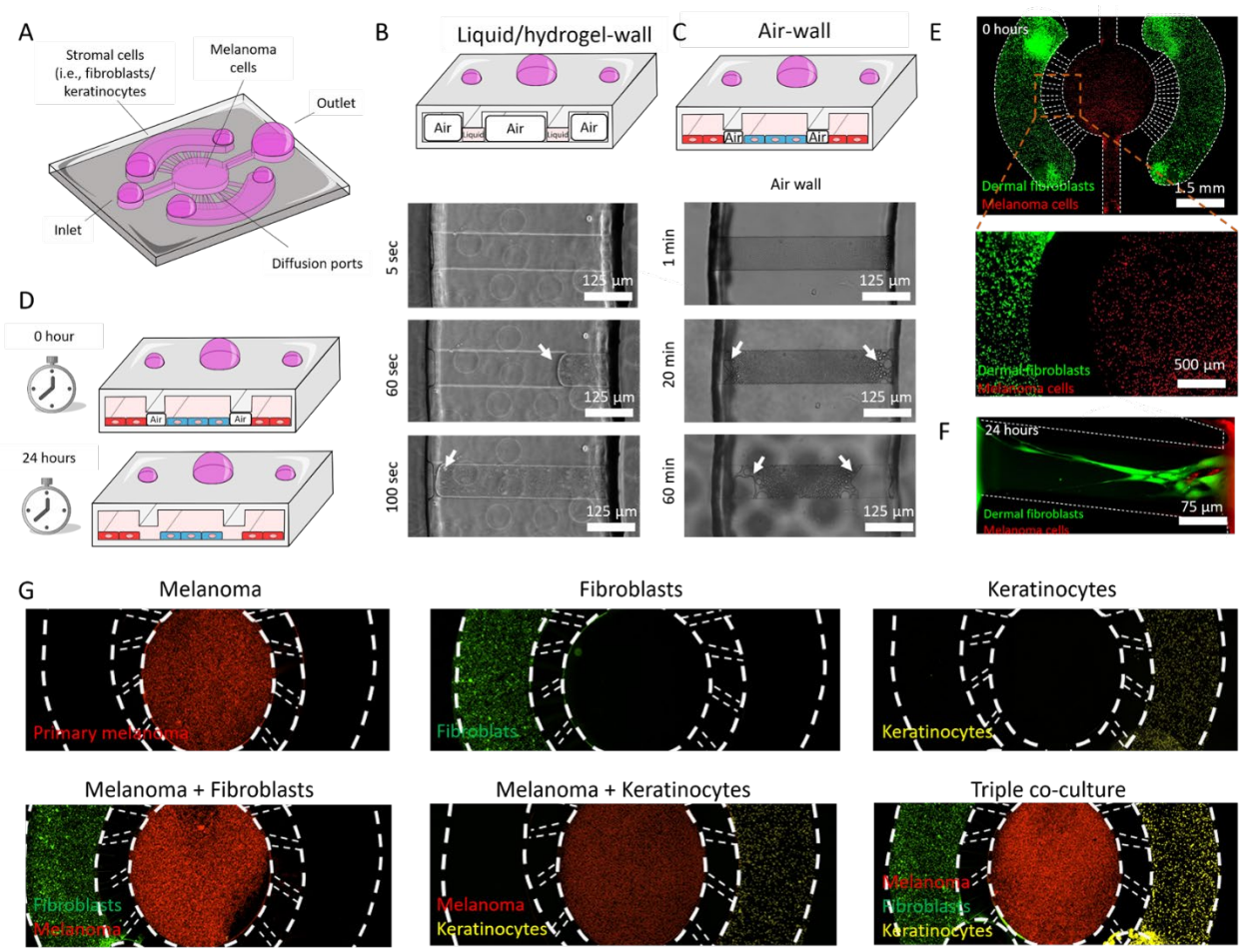


**Figure 1. Microdevice design and air-wall confinement.** A) Scheme depicting the PDMS-based microfluidic device containing the central chamber and two lateral chambers on the sides, connected by a series of concentric narrow microchannels. B) Brightfield time-lapse images showed the evaporation kinetics of liquid-walls. Microdevices were treated with oxygen plasma to render them hydrophilic and ensure the collagen solution flowed through all the chambers and connection microchannels. Next, the collagen solution was aspirated from the lateral and central chambers, leaving the collagen solution confined inside the connection microchannels (upper panel). Given the small volume contained inside the microchannels, the hydrogel solution rapidly evaporated in 2 min (mid- and lower- panel). C and D) Time-lapse images showing the dynamics of the air-wall dissolving. Microdevices were not treated with plasma, to ensure the liquid injected in the lateral and central chambers did not enter the connecting microchannels, generating an air-wall inside these microchannels. The air-wall took several hours to completely dissolve in 10µm-height microchannels, providing the cells enough time to attach to the bottom of the chambers before physically connecting them. E) Melanoma cells and dermal fibroblasts (stained in red and green) were confined in the central and lateral chambers respectively using air-walls. F) After 24 hours, the air-wall was completely dissolved, and cells started to migrate through the connecting microchannels. G) Fluorescence microscopy images showed the confinement achieved by the air-wall method. Melanoma cells, dermal fibroblasts, and keratinocytes were labelled in red, green, and infra-red (shown in yellow) respectively.

## Stromal cell crosstalk induced changes on melanoma cell morphology

Stromal cells such as keratinocytes and dermal fibroblasts surround melanoma cells and have the potential to modify primary tumor evolution and progression. Thus, we co-cultured primary melanoma cells in the presence of dermal fibroblasts and keratinocytes leveraging the air-wall confinement method. Melanoma cells were stained with a red-fluorescent cell tracker and after 3 days in the microdevices, cells were visualized by fluorescence microscopy (Figure 2A). The microscopy images revealed that when cultured in monoculture, melanoma cells formed multicellular clusters with multiple cells grouped together (Figure 2B). On the other hand, when keratinocytes or dermal fibroblasts were present, melanoma cells changed their morphology and transition to a single cell phenotype. The morphological analysis demonstrated that in monoculture, melanoma cells exhibited a circular-like shape (i.e., low aspect ratio), whereas in the presence of dermal fibroblasts or keratinocytes they became more elongated, exhibit a spindle-like morphology (Figure 2C).

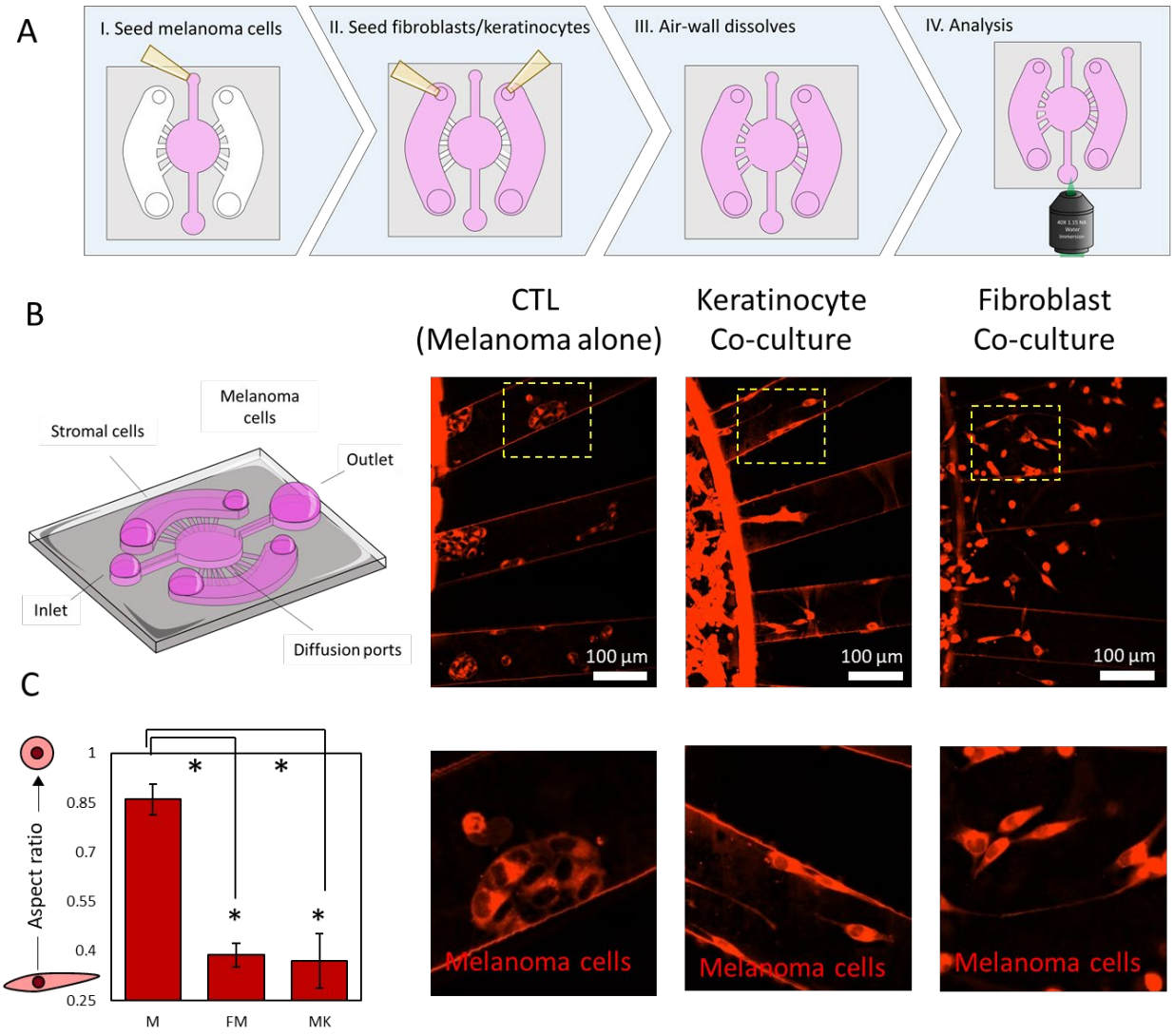


**Figure 2 Morphological analysis.** A) Scheme illustrating the experimental protocol: melanoma cells were confined in the central chamber using the air-wall method with/without dermal fibroblasts/keratinocytes in the lateral chambers. After 3 days in culture, the microdevices were imaged to visualize cell migration and morphology. B) Fluorescence microscopy images showed melanoma cells stained in red after 3 days in culture in monoculture (control condition) and in the presence of fibroblasts, or keratinocytes, or both in the lateral chambers. When cultured alone, melanoma cells formed multicellular clusters. When cultured in the presence of fibroblasts, keratinocytes, or both, melanoma cells spread and appeared as isolated cells. C) Melanoma cell aspect ratio in monoculture and in the presence of dermal fibroblasts and keratinocytes. Asterisks denote p-value<0.05.

Next, we set out to evaluate the molecular crosstalk between dermal fibroblasts, keratinocytes, and melanoma cells. We confined the three cell populations in the microdevice and after 3 days in culture we analyzed secretion of selected chemokines and growth factors (Figure 3A). Presence of fibroblasts, keratinocytes, or both, led to significant changes in chemokine secretion (Figure 3B). More specifically, keratinocytes alone secreted higher levels of IL-6, which were

further increased in the triple co-culture with fibroblasts and melanoma cells. IL-6 is a pleiotropic chemokine produced by multiple cell types including melanoma cells and keratinocytes and dermal fibroblasts in response to inflammation or UV exposure. In melanoma, IL-6 has been shown to decrease tumor apoptosis and increase tumor cell proliferation in more advanced stages[25, 26].

Our analysis also revealed increased IL-8 secretion in the context of coexistence of the three cell types. IL-8 has been also associated with increased melanoma invasion, and metastatic potential. Additionally, IL-8 also regulates tumor-induced angiogenesis[27, 28]. Exposure to UV light leads to overexpression of IL-8 in melanoma cells which in turn accelerates tumor growth. In the co-culture conditions, we observed higher amounts of IL-8, but the levels were not significantly higher than the sum of the fibroblasts, keratinocyte, and melanoma mono-culture conditions combined. However, the observations that keratinocytes and dermal fibroblasts secreted IL-8 suggested their tumor-promoting role in melanoma evolution. IL-1β is an immunomodulatory chemokine secreted by multiple immune cells in response to inflammatory signals[29]. In normal conditions, IL-1β contributes to resolving the last steps of the inflammatory response. However, during the chronic inflammation-like environment within the tumor, IL-1β promotes tumor growth and metastasis by multiple mechanisms such as NF-κB, MAPK, AKT, and WNT pathways[29]. Additionally, IL-1β induces the secretion of other chemokines including the IL-1 family which plays a critical role in tumor progression. In this context, we also observed that keratinocytes secreted high levels of IL-1α. Secretion of IL-1α represses the expression of the transcription factor MITF-M, which controls melanocyte differentiation. Accordingly, IL-1α contributes to maintaining undifferentiated state in melanoma cells, which contributes to tumor growth. Additionally, IL-1α decreases the generation of immunogenic antigens, contributing to an immunosuppressive microenvironment within the tumor[30]. Additionally, IL-1α decreases the redox state of melanoma cells and induces the generation of reactive oxygen species (ROS), which in turn also contribute to maintaining a tumor-promoting inflammatory response[29]. These results suggested dermal fibroblasts, and especially keratinocytes, may be playing a tumor-promoting role. However, keratinocytes also secreted IP-10 and MCP-1, which may help to control tumor growth. IP-10 is an angiostatic factor that has shown a potent antiangiogenic effect[31]. In vivo studies using melanoma models overexpressing IP-10 showed that the tumors had lower microvascular density, slower tumor proliferation and increased apoptosis. However, the exact molecular mechanisms controlling this response remain poorly understood. Recent studies suggested that IP-10-induced angiostatic effects are mediated through the CXCR3 pathway, which has been associated with lymph node metastasis in melanoma[32]. On the other hand, our experiments also revealed that fibroblasts, melanoma cells,

and keratinocytes secreted MCP-1, which has been associated with immune regulation[33]. The co-culture of melanoma cells with fibroblasts and/or keratinocytes showed an additive effect rather than synergistic regarding MCP-1 secretion. MCP-1 is a chemoattractant protein that primarily recruits macrophages to the tumor microenvironment[34]. In melanoma, macrophages can play a dual role, promoting or inhibiting tumor growth depending on other co-stimulatory factors present in the surrounding microenvironment. Interestingly, studies have shown that macrophages attracted by MCP-1 can lead to tumor formation in non-tumorigenic lesions[35]. Altogether, our data highlight the complex interactions between primary melanoma cells and skin microenvironment, specifically due to the surrounding keratinocytes and dermal fibroblasts, which can control melanoma transition from localized primary stage to an invasive tumor and metastatic disease. Identification of the key pathways controlling such transitions might lead to new successful therapies to prevent and treat melanoma.

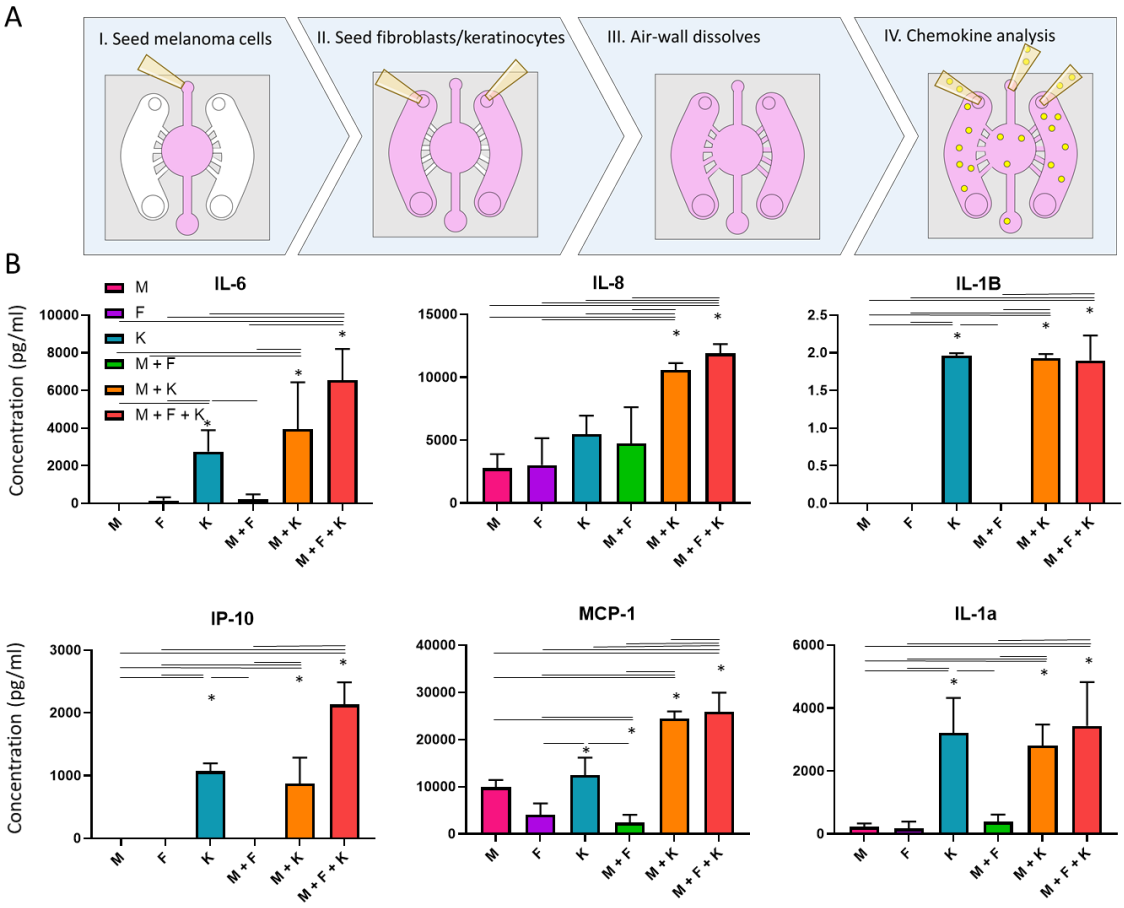

**Figure 3. Cellular crosstalk.** A) Melanoma cells were seeded in the central chamber alone or with dermal fibroblasts and/or keratinocytes on the lateral chambers. After 3days, chemokine secretion was analyzed by MAGPIX. C) Bar graphs showed the chemokine secretion in melanoma cells alone (M), dermal fibroblasts alone (F), keratinocytes alone (K), melanoma with dermal fibroblasts (M + F), melanoma cells and keratinocytes (M + K), and the triple co-culture (M + F + K). Asterisks denote p-value<0.05.

## Cell metabolism

Tumor cells exhibit higher proliferation rates compared with normal cells, which forces them to adapt their metabolism to satisfy the high demand of carbohydrates, amino acids, and fatty acids[36]. Altered tumor metabolism offers opportunity to selectively destroy cancer cells without damaging the normal tissue[37]. Therefore, we compared cell metabolism in melanoma cells, dermal fibroblasts, and keratinocytes using optical metabolic imaging (OMI). OMI relies on the use of multi-photon microscopy to visualize the autofluorescence of NAD(P)H and FAD, molecules involved in cell metabolism and cell redox balance (Figure 4A)[38]. Rapidly proliferating cells, such as cancer cells, commonly rely on glycolysis to generate "building blocks" to support cell proliferation, generating an excess of NAD(P)H as a by-product of their anaerobic metabolism[36]. Therefore, we quantified NAD(P)H autofluorescence intensity and divided by the FAD autofluorescence intensity to calculate the normalized redox ratio (Figure 4B and C). The NAD(P)H/FAD ratio has been used in previous studies to monitor cellular redox potential in live cells without any external labeling agent[24, 38, 39]. When cultured alone, melanoma cells exhibited a higher redox ratio compared with dermal fibroblasts and keratinocytes (i.e., normal cells). Interestingly, the co-culture with keratinocytes, dermal fibroblasts, or both, led to a significant change in melanoma cell redox ratio, suggesting a metabolic shift in melanoma cells.

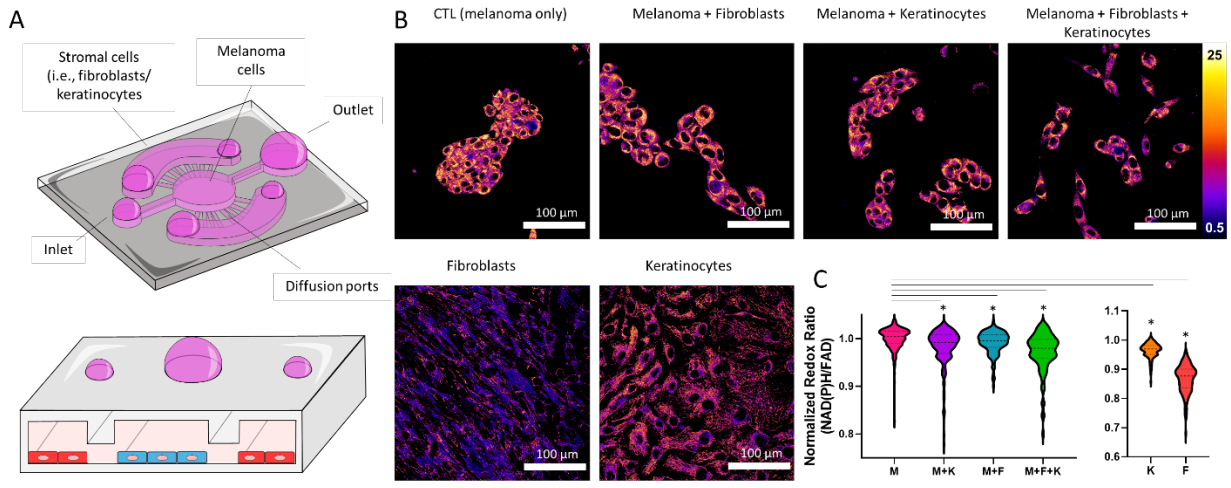

**Figure 4. Optical metabolic imaging.** A) Schematic representation of the triple co-culture inside the microdevice, including melanoma cells, dermal fibroblasts, and keratinocytes. B) Melanoma cells were imaged by multi-photon microscopy. Images shows normalized ratio of NAD(P)H autofluorescence divided by FAD autofluorescence, defined as normalized redox ratio. Melanoma cells were imaged alone and in the presence of dermal fibroblasts and/or keratinocytes. Images of fibroblasts and keratinocytes alone are also shown. C) Right panel shows normalized redox ratio of melanoma cells alone and in the co-culture conditions. Left panel shows normalized redox ratio of dermal fibroblasts and keratinocytes alone. Asterisk denotes a p-value<0.05.

Additionally, we analyzed NAD(P)H fluorescence lifetime (NAD(P)H $\tau_m$) in melanoma cells, dermal fibroblasts, keratinocytes, and multiple combinations (Figure 5). NAD(P)H $\tau_m$ is modulated by the ratio of NAD(P)H free in the cytoplasm to the amount bound to enzymes (e.g., mitochondrial respiratory complexes). Thus, an increase in NAD(P)H $\tau_m$ is associated with an increase in the ratio NAD(P)H-bound vs NAD(PH)-free, which commonly happens during oxidative phosphorylation. Our results demonstrated that melanoma cells had a higher NAD(P)H $\tau_m$ compared with normal cells such as dermal fibroblasts and keratinocytes, demonstrating again the different metabolic phenotype exhibited by melanoma cells. Interestingly, when co-cultured with dermal fibroblasts, keratinocytes, or both, melanoma cells showed a decrease in their NAD(P)H $\tau_m$, which agrees with an increase in the amount of NAD(P)H free in the cytoplasm. These results are consistent with the chemokine analysis (i.e., secretion of tumor-promoting chemokines), suggesting dermal fibroblasts and keratinocytes play a tumor-supporting role. Enabled by this platform, in-depth proteomics, and metabolomics analysis (e.g., mass spectrometry) could pinpoint the specific molecular alterations driving tumor-stroma crosstalk and melanoma progression.

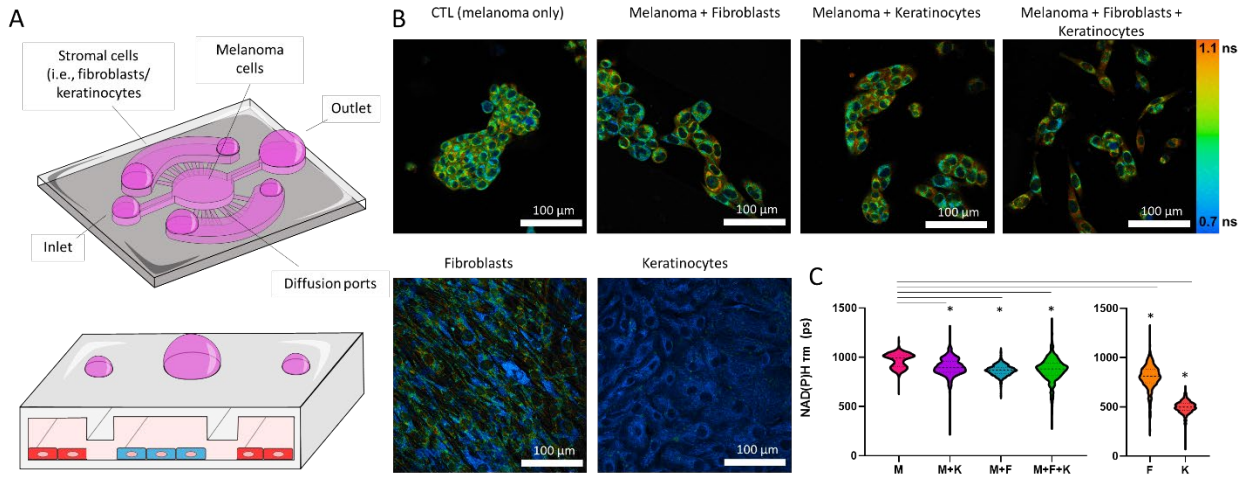


**Figure 5 NAD(P)H FLIM.** A) Schematic representation of the triple co-culture inside the microdevice, including melanoma cells, dermal fibroblasts, and keratinocytes. B) Melanoma cells imaged by multi-photon microscopy. Images show NAD(P)H FLIM. Melanoma cells were imaged alone and in the presence of dermal fibroblasts and/or keratinocytes. Images of fibroblasts and keratinocytes alone are also shown. C) Right panel shows melanoma cell NAD(P)H FLIM alone and in the co-culture conditions. Left panel shows keratinocyte and dermal fibroblast NAD(PH) FLIM. Asterisk denotes a p-value<0.05.

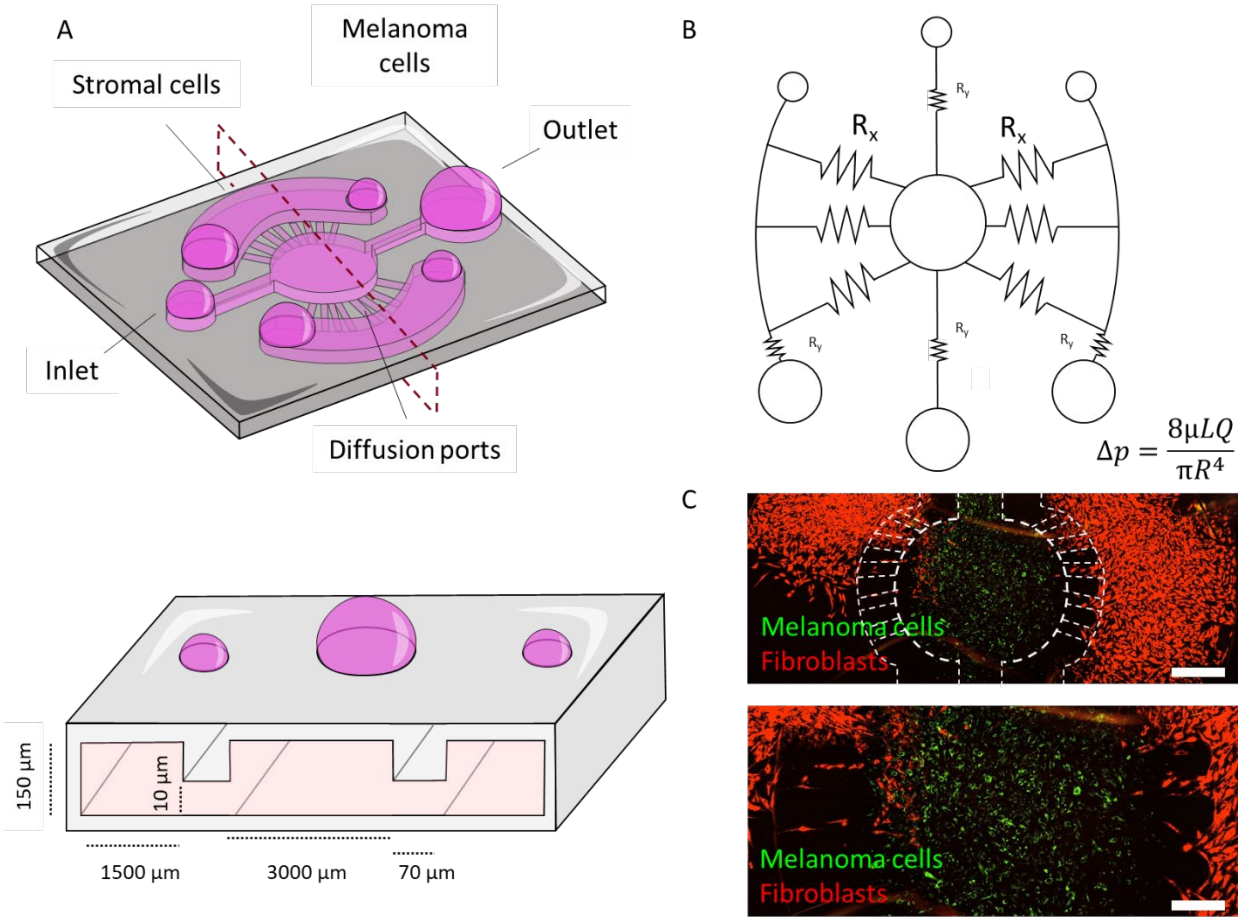


**Supporting Figure 1.** Cell confinement based on fluidic resistance. A) Microdevice scheme. The connection microchannels present a smaller cross-section compared with central channel connecting with the central microchamber. B) Schematic representation of the microdevice demonstrating the difference in fluidic resistance generated by the connection microchannels compared with the path defined by the central chamber and central channel. Bottom right shows the Hagen–Poiseuille equation where Δp is the pressure difference between the two ends, μ is the dynamic viscosity, L is the length of the channel, Q is volumetric flow rate, and R is the radius of the channel. C) Confocal image showing the confinement achieved by fluidic resistance using melanoma cells (in green) and dermal fibroblasts (in red). Fibroblasts can be observed inside the central chamber, demonstrating the presence of crossflow from the lateral chambers towards the central chamber.

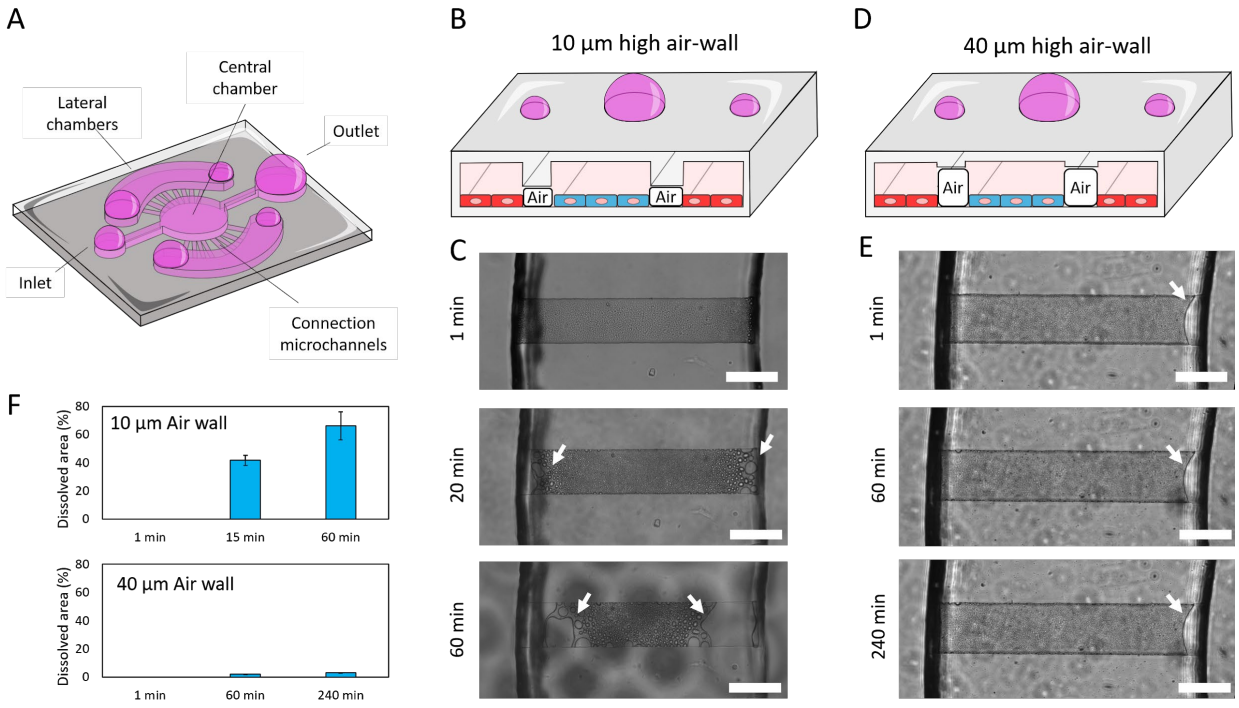


**Supporting Figure 2 Effect of air volume on the air-wall dynamics.** A) Scheme of the microdevice design. B) Schematic representation of a microdevice designed with 10µm-height connection microchannels. C) 60 minutes time-lapse images showing the air-wall dissolving. After 60 minutes, 65% of the air-wall appeared to be dissolved, observing droplets of different sizes (white arrows). D) Schematic representation of a microdevice designed with 40µm-height connection microchannels. E) 240 minutes time-lapse images showing less than 5% of the air-wall dissolving. F) Bar graph showed the percentage of air-wall dissolved at different time-points in the 10 and 40µm-height air-wall microdevices. The results demonstrate the effect of the air-wall height in the dissolving dynamics.

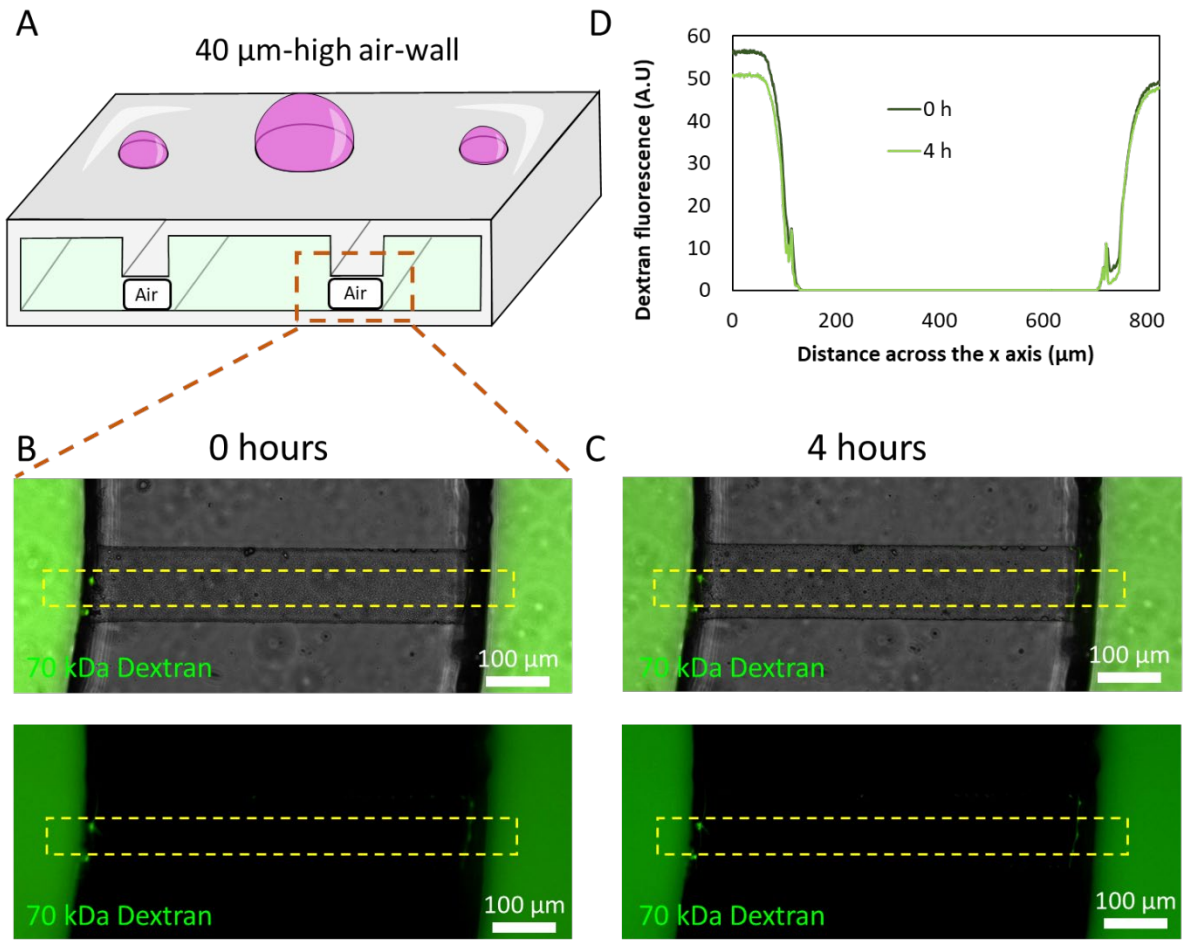


**Supporting Figure 3. Air-walls prevent molecular diffusion.** A) Schematic showing a 40µm-high air-wall separating a 10µM fluorescent 70kDa-dextran solution. The dextran solution was perfused in the central and lateral chambers, generating an air-wall in the connection channel. B-C) Fluorescence microscopy images showing dextran fluorescence at 0 and 4 hours post-dextran injection. D) Graph analyzed the fluorescent profile across the delimited region in B and C (i.e., yellow rectangle). The profile showed no dextran diffusion across the connection channel after 4 hours in culture.

## Conclusion

Melanoma progression is a complex process that is influenced by both primary melanoma cell intrinsic mechanisms and tissue microenvironment, specifically epidermal keratinocytes and dermal fibroblasts. Fibroblasts and keratinocytes may play a dual role, supporting or inhibiting tumor growth depending on the specific mutational and environmental landscape (e.g., BRAF mutations, hypoxia). Therefore, *in vitro* tools that allow investigation of the cross-talk between these cell types might accelerate the identification of successful therapies against melanoma. Here, we presented a methodology to control cell patterning in microfluidic in vitro platforms without the need for external equipment, porous membranes, or hydrogels. Our protocol relied on the use of air-walls to confine the different cell populations in adjacent microfluidic chambers. Once the multiple cell populations were attached, these air-walls spontaneously dissolved in a predictable fashion, allowing cellular crosstalk and migration. The time needed to dissolve these air-walls was controlled by adjusting the air-wall volume, which allows a precise control over their co-culture conditions. This methodology allowed us to study the effects of dermal fibroblasts and keratinocytes on primary melanoma cells. Our results demonstrated that the co-culture with fibroblasts, keratinocytes, or both, led to significant changes in melanoma cell morphology, secretion pattern, and metabolic phenotype. Thus, the use of air-walls could provide a versatile tool to accelerate the identification of new therapies targeting tumor crosstalk.

## Acknowledgments

This work was supported by Department of Defense grant W81XWH-18-PRCRP-IASF (CA181014) and in part by UW Skin Disease Research Center grant (NIH P30 P30AR066524), US Veterans Affairs grant (I01 BX004921), NIH grants R01 CA164492, R01 CA185747, R01 CA205101, and NSF grant CBET-1642287.University of Wisconsin Carbone Cancer Center (AAB7173) and Morgridge Research Institute.

## References

1. C. m. a. C. w. https://www.cancer.org/cancer/melanoma-skin-cancer/about/key-statistics.html#:~:text=How%20common%20is%20melanoma%3F, (accessed 2020-09-03).

2. https://www.cancer.org/research/cancer-facts-statistics/all-cancer-facts-figures/cancer-facts-figures-2020.html, (accessed 2020-09-03).
3. A. Vultur and M. Herlyn, *Cancer cell*, 2013, **23**, 706-706 e701.
4. C. Gaggioli and E. Sahai, *Pigment cell research*, 2007, **20**, 161-172.
5. W. E. Damsky and M. Bosenberg, *Oncogene*, 2017, **36**, 5771-5792.
6. L. Zhou, K. Yang, T. Andl, R. R. Wickett and Y. Zhang, *Journal of Cancer*, 2015, **6**, 717-726.
7. J. X. Wang, M. Fukunaga-Kalabis and M. Herlyn, *Journal of cell communication and signaling*, 2016, **10**, 191-196.
8. J. W. Van Kilsdonk, M. Bergers, L. C. Van Kempen, J. Schalkwijk and G. W. Swart, *Melanoma research*, 2010, **20**, 372-380.
9. E. H. Flach, V. W. Rebecca, M. Herlyn, K. S. Smalley and A. R. Anderson, *Mol Pharm*, 2011, **8**, 2039-2049.
10. J. M. Ayuso, M. Virumbrales-Munoz, P. H. McMinn, S. Rehman, I. Gomez, M. R. Karim, R. Trusttchel, K. B. Wisinski, D. J. Beebe and M. C. Skala, *Lab on a chip*, 2019, **19**, 3461-3471.
11. K. H. Benam, R. Villenave, C. Lucchesi, A. Varone, C. Hubeau, H. H. Lee, S. E. Alves, M. Salmon, T. C. Ferrante, J. C. Weaver, A. Bahinski, G. A. Hamilton and D. E. Ingber, *Nature methods*, 2016, **13**, 151-157.
12. D. T. T. Phan, X. Wang, B. M. Craver, A. Sobrino, D. Zhao, J. C. Chen, L. Y. N. Lee, S. C. George, A. P. Lee and C. C. W. Hughes, *Lab on a chip*, 2017, **17**, 511-520.
13. J. M. Ayuso, H. A. Basheer, R. Monge, P. Sanchez-Alvarez, M. Doblare, S. D. Shnyder, V. Vinader, K. Afarinkia, L. J. Fernandez and I. Ochoa, *Plos One*, 2015, **10**, e0139515.
14. G. Adriani, D. Ma, A. Pavesi, E. L. K. Goh and R. D. Kamm, *Ieee Eng Med Bio*, 2015, 338-341.
15. K. J. Jang, A. P. Mehr, G. A. Hamilton, L. A. McPartlin, S. Chung, K. Y. Suh and D. E. Ingber, *Integrative biology : quantitative biosciences from nano to macro*, 2013, **5**, 1119-1129.
16. J. Deng, W. Wei, Z. Chen, B. Lin, W. Zhao, Y. Luo and X. Zhang, *Micromachines*, 2019, **10**.
17. S. Jalili-Firoozinezhad, F. S. Gazzaniga, E. L. Calamari, D. M. Camacho, C. W. Fadel, A. Bein, B. Swenor, B. Nestor, M. J. Cronce, A. Tovaglieri, O. Levy, K. E. Gregory, D. T. Breault, J. M. S. Cabral, D. L. Kasper, R. Novak and D. E. Ingber, *Nature biomedical engineering*, 2019, **3**, 520-531.
18. J. S. Jeon, S. Bersini, M. Gilardi, G. Dubini, J. L. Charest, M. Moretti and R. D. Kamm, *Proceedings of the National Academy of Sciences of the United States of America*, 2015, **112**, 214-219.
19. V. S. Shirure, Y. Bi, M. B. Curtis, A. Lezia, M. M. Goedegebuure, S. P. Goedegebuure, R. Aft, R. C. Fields and S. C. George, *Lab on a chip*, 2018, **18**, 3687-3702.
20. V. van Duinen, A. van den Heuvel, S. J. Trietsch, H. L. Lanz, J. M. van Gils, A. J. van Zonneveld, P. Vulto and T. Hankemeier, *Sci Rep*, 2017, **7**, 18071.
21. C. Kim, J. Kasuya, J. Jeon, S. Chung and R. D. Kamm, *Lab on a chip*, 2015, **15**, 301-310.
22. A. Pavesi, A. T. Tan, S. Koh, A. Chia, M. Colombo, E. Antonecchia, C. Miccolis, E. Ceccarello, G. Adriani, M. T. Raimondi, R. D. Kamm and A. Bertoletti, *Jci Insight*, 2017, **2**.
23. C. Pak, N. S. Callander, E. W. Young, B. Titz, K. Kim, S. Saha, K. Chng, F. Asimakopoulos, D. J. Beebe and S. Miyamoto, *Integrative biology : quantitative biosciences from nano to macro*, 2015, **7**, 643-654.
24. J. M. Ayuso, A. Gillette, K. Lugo-Cintron, S. Acevedo-Acevedo, I. Gomez, M. Morgan, T. Heaster, K. B. Wisinski, S. P. Palecek, M. C. Skala and D. J. Beebe, *EBioMedicine*, 2018, **37**, 144-157.
25. L. Hoejberg, L. Bastholt and H. Schmidt, *Melanoma research*, 2012, **22**, 327-333.
26. R. Kucera, O. Topolcan, I. Treskova, J. Kinkorova, J. Windrichova, R. Fuchsova, S. Svobodova, V. Treska, V. Babuska, J. Novak and J. Smejkal, *Anticancer research*, 2015, **35**, 3537-3541.
27. K. Norrby, *Cell proliferation*, 1996, **29**, 315-323.
28. S. K. Srivastava, A. Bhardwaj, S. Arora, N. Tyagi, A. P. Singh, J. E. Carter, J. G. Scammell, O. Fodstad and S. Singh, *British journal of cancer*, 2015, **112**, 1772-1781.

29. R. Bent, L. Moll, S. Grabbe and M. Bros, *International journal of molecular sciences*, 2018, **19**.
30. O. Kholmanskikh, N. van Baren, F. Brasseur, S. Ottaviani, J. Vanacker, N. Arts, P. van der Bruggen, P. Coulie and E. De Plaen, *Int J Cancer*, 2010, **127**, 1625-1636.
31. J. Yang and A. Richmond, *Mol Ther*, 2004, **9**, 846-855.
32. K. Kawada, M. Sonoshita, H. Sakashita, A. Takabayashi, Y. Yamaoka, T. Manabe, K. Inaba, N. Minato, M. Oshima and M. M. Taketo, *Cancer Res*, 2004, **64**, 4010-4017.
33. T. Yoshimura, *Cellular & molecular immunology*, 2018, **15**, 335-345.
34. Y. Nakasone, M. Fujimoto, T. Matsushita, Y. Hamaguchi, D. L. Huu, M. Yanaba, S. Sato, K. Takehara and M. Hasegawa, *The American journal of pathology*, 2012, **180**, 365-374.
35. M. Nesbit, H. Schaider, T. H. Miller and M. Herlyn, *J Immunol*, 2001, **166**, 6483-6490.
36. M. A. Keibler, T. M. Wasylenko, J. K. Kelleher, O. Iliopoulos, M. G. Vander Heiden and G. Stephanopoulos, *Cancer & metabolism*, 2016, **4**, 16.
37. *Nat Rev Drug Discov*, 2010, **9**, 503-504.
38. A. J. Walsh, R. S. Cook, M. E. Sanders, L. Aurisicchio, G. Ciliberto, C. L. Arteaga and M. C. Skala, *Cancer Res*, 2014, **74**, 5184-5194.
39. A. J. Walsh, R. S. Cook, H. C. Manning, D. J. Hicks, A. Lafontant, C. L. Arteaga and M. C. Skala, *Cancer Res*, 2013, **73**, 6164-6174.